Tumor necrosis factor stimulates fibroblast growth factor 23 levels in chronic kidney disease and non-renal inflammation

Egli-Spichtig, Daniela ; Imenez Silva, Pedro Henrique ; Glaudemans, Bob ; Gehring, Nicole ; Bettoni, Carla ; Zhang, Martin Y H ; Pastor-Arroyo, Eva M ; Schönenberger, Désirée ; Rajski, Michal ; Hoogewijs, David ; Knauf, Felix ; Misselwitz, Benjamin ; Frey-Wagner, Isabelle ; Rogler, Gerhard ; Ackermann, Daniel ; Ponte, Belen ; Pruijm, Menno ; Leichtle, Alexander ; Fiedler, Georg-Martin ; Bochud, Murielle ; Ballotta, Virginia ; Hofmann, Sandra ; Perwad, Farzana ; Föller, Michael ; Lang, Florian ; Wenger, Roland H ; Frew, Ian ; Wagner, Carsten A

Abstract: Fibroblast growth factor 23 (FGF23) regulates phosphate homeostasis, and its early rise in patients with chronic kidney disease (CKD) is independently associated with all-cause mortality. Since inflammation is characteristic of CKD and associates with increased plasma FGF23 we examined whether inflammation directly stimulates FGF23. In a population-based cohort, plasma tumor necrosis factor (TNF) was the only inflammatory cytokine that independently and positively correlated with plasma FGF23. Mouse models of CKD showed signs of renal inflammation, renal FGF23 expression and elevated systemic FGF23 levels. Renal FGF23 expression coincided with expression of the orphan nuclear receptor Nurr1 regulating FGF23 in other organs. Antibody-mediated neutralization of TNF normalized plasma FGF23 and suppressed ectopic renal Fgf23 expression. Conversely, TNF administration to control mice increased plasma FGF23 without altering plasma phosphate. Moreover, in Il10-deficient mice with inflammatory bowel disease and normal kidney function, plasma FGF23 was elevated and normalized upon TNF neutralization. Thus, the inflammatory cytokine TNF contributes to elevated systemic FGF23 levels and also triggers ectopic renal Fgf23 expression in animal models of CKD.

DOI: https://doi.org/10.1016/j.kint.2019.04.009

Antibody mediated TNF neutralization decreases FGF23 levels in animal models of chronic kidney disease and non-renal inflammation

Daniela Egli-Spichtig[1,2#], Pedro Henrique Imenez Silva[1#], Bob Glaudemans[1], Nicole Gehring[1], Carla Bettoni[1], Martin Zhang[2], Eva Pastor Arroyo[1], Désirée Schönenberger[1], Michal Rajski[1], David Hoogewijis[1], Felix Knauf[3], Benjamin Misselwitz[4], Isabelle Frey-Wagner[4], Gerhard Rogler[4], Daniel Ackermann[5], Belen Ponte[6], Menno Pruijm[7], Alexander Leichtle[8], Georg-Martin Fiedler[8], Murielle Bochud[9], Sandra Hofmann Boss[10], Farzana Perwad[2], Michael Föller[10], Florian Lang[11], Roland H. Wenger[1], Ian Frew[1], Carsten A. Wagner[1]*

# contributed equally to the manuscript

[1]Institute of Physiology, University of Zurich, Zurich, Switzerland and National Center of Competence in Research NCCR Kidney.CH, Switzerland
[2]Department of Pediatrics, Division of Nephrology, University of California San Francisco, San Francisco, California, United States of America
[3]Division of Nephrology, Charité - Universitätsmedizin Berlin, Berlin, Germany
[4]University Hospital Zurich, Clinic for Gastroenterology and Hepatology, Zürich, Switzerland
[5]Department of Nephrology and Hypertension, Inselspital, Bern University Hospital and University of Bern, Switzerland
[6]Department of Nephrology, University Hospital of Geneva (HUG), Switzerland
[7]Department of Nephrology, Lausanne University Hospital (CHUV), Switzerland
[8]Institute of Clinical Chemistry, Inselspital, Bern University Hospital, University of Bern, Switzerland.
[9]Institute of Social and Preventive Medicine (IUMSP), Lausanne University Hospital (CHUV), Switzerland
[10]Department of Biomedical Engineering and Institute for Complex Molecular Systems, Eindhoven University of Technology, P.O. Box 513, 5600 MB Eindhoven, The Netherlands
[11]Martin-Luther-Universität Halle-Wittenberg, Ernährungsphysiologie - Halle/S. Germany
[12]Institute of Physiology I, University of Tübingen, Germany

*** Corresponding author**

Carsten A. Wagner
Institute of Physiology
University of Zurich
Winterthurerstrase 190
CH-8057 Zurich
Switzerland
Phone: +41-44-63 55023
Fax: +41-44-63 56814
Email: Wagnerca@access.uzh.ch

Abstract

Fibroblast growth factor 23 (FGF23) regulates phosphate homeostasis and its early rise in patients with chronic kidney disease (CKD) is independently associated with all-cause mortality. Since inflammation is characteristic for CKD and has been associated with plasma FGF23 we examined whether inflammation directly stimulates FGF23. In a population-based cohort, plasma tumor necrosis factor (TNF) was the only inflammatory cytokine that independently and positively correlated with plasma FGF23. Mouse models of CKD showed signs of renal inflammation, renal FGF23 expression and elevated systemic FGF23. Renal FGF23 expression coincided with expression of the orphan nuclear receptor Nurr1 regulating FGF23 in other organs. Antibody-mediated neutralization of TNF normalized plasma FGF23 and ectopic renal *Fgf23* expression. Conversely, TNF administration to control mice increased plasma FGF23 without altering plasma phosphate. Similarly, in *Il10* deficient mice with inflammatory bowel disease and normal kidney function, FGF23 was elevated and normalized upon TNF neutralization. In conclusion, the inflammatory cytokine TNF contributes to elevated systemic FGF23 levels and triggers also ectopic renal *Fgf23* expression in CKD animal models.

Keywords

Fibroblast growth factor 23 (FGF23), tumor necrosis factor (TNF), chronic kidney disease (CKD), inflammation, cytokine, inflammatory bowel disease, bone.

INTRODUCTION

Chronic kidney disease (CKD) causes a severe disturbance of mineral metabolism, one of the leading factors for morbidity and mortality in patients with end stage renal disease (ESRD) [1, 2]. Fibroblast growth factor 23 (FGF23) increases early during CKD progression and is required to maintain serum phosphate levels while kidney function declines [3]. In CKD patients, high FGF23 levels are associated with an increased risk of mortality independent of plasma phosphate [4]. FGF23 promotes left ventricular hypertrophy in rodents [5] and elevated FGF23 is a risk factor in the general population for all-cause and cardiovascular mortality [6].

FGF23 is critical for the regulation of phosphate homeostasis and vitamin D_3 metabolism [7]. The main target organ of FGF23 is the kidney where FGF23 binds together with αKlotho to FGF receptors and inhibits phosphate reabsorption and decreases 1,25-$(OH)_2$ vitamin D_3 (1,25$(OH)_2$D) [8, 9]. FGF23 levels are regulated by a variety of stimuli including calcitriol, PTH, insulin, aldosterone, erythropoietin, and adipokinines [8, 10-13]. Moreover, FGF23 may be linked to inflammation. In the *Chronic Renal Insufficiency Cohort* elevated FGF23 is independently associated with higher IL-6 and TNF [14] and also in a smaller cohort with only 103 CKD patients, RANTES and IL-12 associated with higher FGF23 [15]. The association between FGF23 and inflammation markers is not limited to CKD. *The Reasons for Geographic and Racial Differences in Stroke* study found a positive correlation of FGF23 with IL-6 and IL-10 in a non-CKD population [16]. Children during an acute phase of inflammatory bowel disease (IBD) had elevated FGF23 that normalized in the remission phase [17]. Furthermore, chondrocytes from patients with osteoarthritis have elevated *Fgf23* gene expression [18]. Microarray data from mouse models with FGF23 excess (*Col4a3* KO, *Hyp*, and *Fgf23* transgenic mice) show an activation of genes important in the regulation of the inflammatory response such as transforming growth factor beta (TGFβ), tumor necrosis factor (TNF) and nuclear factor of kappa light polypeptide gene enhancer in B-cells (NFκB) [19]. Further, inflammatory stimuli and the hypoxia inducible transcription factor HIF-1 enhance FGF23 expression: TNF and TGFβ2

increases FGF23 expression in bone cells *in vitro* and HIF-1, interleukin-1 beta (IL-1β), lipopolysaccharide (LPS) increase FGF23 expression *in vitro* and *in vivo* [20-25]. Also, in an obesity induced model, TNF is necessary for the increase in FGF23 levels [26]. Some inflammatory stimuli, including TNF, may act on *Fgf23* transcription via a 16 kb enhancer element [27]. Moreover, in the folic-acid induced AKI model as well as in the adenine CKD model, genetic ablation of Il-6 reduced the increase in FGF23 [28]. Thus, inflammatory cytokines may play an important role at least in the early phase of CKD to induce FGF23. However, whether TNF is a critical player has not been demonstrated.

Here, we investigated the association between inflammatory cytokines with plasma FGF23 in a population-based cohort and evaluated the effect of TNF on the regulation of plasma FGF23 in CKD animal models and in a non-renal inflammation model. Furthermore, we evaluated the role of hypoxia on *Fgf23* gene expression. Our results demonstrate a critical role for TNF to stimulate FGF23 in models of renal and non-renal inflammatory diseases.

Results

Plasma TNF positively correlated with intact FGF23 in the SKIPOGH population based cohort

The *Swiss Kidney Project on Genes in Hypertension* (SKIPOGH) is a family and population-based, multicenter, cross-sectional study including 1131 subjects randomly selected [29]. We assessed the relationship between plasma intact FGF23 (iFGF23) and parameters of phosphate metabolism, inflammatory cytokines, and iron metabolism while considering familial correlation. Participants with drugs interacting with calcium, magnesium and phosphate metabolism, inflammation and iron metabolism or have diuretic action were excluded. Based on a linear mixed model with family as random effect, $1,25(OH)_2D$, 25-(OH) vitamin D_3 (25(OH)D), TNF and calcium showed the highest fixed effects and were considered significant predictors of plasma iFGF23 while holding all the other variables constant (Figure 1). The standard deviation of the random effect was low compared to the standard deviation of the residuals (0.26 vs 0.93), which means that most of the variation in iFGF23 levels was due to the fixed effects (i.e. hormones, cytokines, etc.). There was no correlation between plasma iFGF23 and plasma phosphate, PTH, or eGFR. Besides TNF, no other inflammatory cytokine such as interferon gamma (IFNγ), IL-1β, IL-6, or IL-10 correlated with plasma iFGF23.

We also analyzed the cohort without applying exclusion criteria based on drugs. $1,25(OH)_2D$, 25(OH)D, and calcium remained as predictors of iFGF23 while phosphate, PTH and eGFR arose as additional predictors of iFGF23 (Figure S1). TNF effect on iFGF23 is reduced in this population.

Inflammation in kidneys of *Pkd1* conditional KO mice

TNF is increased in CKD patients, stimulates FGF23 expression in an osteocyte cell line, and was the only inflammatory cytokine associated with iFGF23 in the SKIPOGH cohort [14, 22, 31, 32]. Thus, we tested in two CKD mouse models whether TNF contributes to the

rise of iFGF23 during the early phase of kidney disease. First, slowly progressing polycystic kidney disease (PKD) was induced in *Pkd1* conditional KO mice [33]. Kidney function and two-kidney per body weight ratio were similar in 6 week old mice whereas kidney function was decreased and two-kidney per body weight ratio was increased in 12 week old *Pkd1*, *cre+* mice (Figure S2). At week 6, iFGF23, TmP/GFR as well as renal *Tnf* and *Tgfb* mRNA expression were similar in $Pkd1^{fl/fl}$, *cre-* and $Pkd1^{fl/fl}$, *cre+* mice (Figure 2 a - d). Progression of kidney disease was accompanied by increased plasma iFGF23, decreased TmP/GFR as well as increased *Tnf* and *Tgfb* mRNA expression in $Pkd1^{fl/fl}$, *cre+* mice (Figure 2 a - d). TNF binding to TNF receptors activates the NFκB signaling pathway. The ratio of phospho-NFκB p65 to total NFκB p65 protein in the nuclear fraction of total kidney was significantly elevated in $Pkd1^{fl/fl}$, *cre+* mice (Figure 2 e). Increased renal inflammatory cytokines in 12 week old $Pkd1^{fl/fl}$, *cre+* mice were paralleled by the appearance of renal *Fgf23* expression and by the upregulation of the osteogenic marker gene *Runx2* (Figure 2 f and S2 e). Bone *Fgf23* and *Runx2* mRNA expression were unchanged (Figure 2 g and S2 f).

TNF blockade in *Pkd1* conditional KO mice suppressed FGF23

The effect of acute TNF blockade on FGF23 expression in PKD kidneys and on plasma iFGF23 was investigated. We injected intraperitoneally (i.p.) a single dose of 0.5 mg anti-TNF antibody or isotypic IgG control into 12 week old $Pkd1^{fl/fl}$, *cre+* and $Pkd1^{fl/fl}$, *cre-* mice. After 24 hours, anti-TNF treated mice had a significant reduction of plasma TNF compared to the IgG control treated mice confirming the efficacy of the anti-TNF antibody (Figure 3 a). There was no difference in plasma TNF between IgG control treated $Pkd1^{fl/fl}$, *cre+* and $Pkd1^{fl/fl}$, *cre-* mice. Importantly, elevated plasma iFGF23 in $Pkd1^{fl/fl}$, *cre+* mice was normalized by anti-TNF but not IgG control treatment (Figure 3 b). Plasma C-terminal FGF23 (cFGF23) was increased in IgG control treated $Pkd1^{fl/fl}$, *cre+* and anti-TNF treaded $Pkd1^{fl/fl}$, *cre-* compared to IgG control treated $Pkd1^{fl/fl}$, *cre-* mice consequently iFGF23/cFGF23 ratio was elevated in IgG control treated $Pkd1^{fl/fl}$, *cre-* mice (Figure S4 a

– c). There was no change in plasma phosphate and urea as well as the abundance of the sodium dependent phosphate co-transporter NaPi-IIa at the brush border membrane (BBM) (Figure 3 c - e). In *Pkd1*$^{fl/fl}$*, cre+* mice, TNF neutralization decreased ectopic renal *Fgf23* mRNA expression while *Fgf23* mRNA expression in bone (Figure 3 f and g) and *Tnf*, and *Tgfb* mRNA expression in kidney (Figure 3 h and i) were unchanged. The mRNA expression of the inflammatory cytokines *Il1b* and *Il6* was elevated in PKD kidneys but did not change with treatment (Figure S3).

The orphan nuclear receptor Nurr1 is downstream of TNF signaling and activates *Fgf23* mRNA expression in rat osteosarcoma cells upon PTH treatment [37, 38]. *Nurr1* mRNA was detected in mouse kidney and bone (Figure S5). In the kidney of 12 week old *Pkd1*$^{fl/fl}$*, cre+* mice, *Nurr1* mRNA expression was upregulated and Nurr1 protein was predominantly localized in the cell nucleus compared to *Pkd1*$^{fl/fl}$*, cre-* mice where Nurr1 was mainly distributed in the cytoplasm (Figure S6). Further, nuclear Nurr1 staining in *Pkd1*$^{fl/fl}$*, cre+* mice was often co-localized with FGF23.

TNF but not hypoxia increased FGF23 levels

We evaluated the effect of systemic TNF administration on plasma iFGF23 therefore we injected wild type mice for two consecutive days with 2 µg recombinant mouse TNF. After 48-hours, plasma iFGF23 increased while cFGF23 and iFGF23/cFGF23 ratio were unchanged (Figure 4a and S4 d – f). Furthermore plasma TNF and fractional excretion of phosphate increased, plasma urea decreased while plasma phosphate and creatinine levels were unchanged (Figure 4 b - f). In bone and spleen *Fgf23* mRNA expression decreased in TNF injected compared to vehicle injected mice whereas *Fgf23* mRNA expression in thymus and bone marrow was unchanged (Figure 4 g -j). We cultured primary osteocytes from tibias and femurs of mice [39, 40] for 2 weeks before being supplemented for 24 hours either with 10 ng/ml TNF or 10 nM $1,25(OH)_2D$. TNF as well as $1,25(OH)_2D$ increased *Fgf23* mRNA expression (Figure 4 k). TNF and $1,25(OH)_2D$ decreased the expression of *Dmp1* (Figure 4 l). Dmp1 inhibits *Fgf23* gene expression

and loss of *DMP1* in patients causes hypophosphatemic rickets due to high FGF23 levels [41]. TNF but not 1,25$(OH)_2$D increased the expression of *Galnt3* and *Nurr1* (Figure 4 m and n). Galnt3 mediates O-glycosylation of FGF23 preventing proteolytic cleavage of FGF23 [42, 43].

CKD kidneys are commonly affected by hypoxia [44, 45] which was recently suggested to stimulate FGF23 expression through the hypoxia inducible transcription factor HIF-1 [20, 21, 24]. We studied in MC3T3-E1 mouse preosteoblasts the effect of hypoxia on *Fgf23* gene expression. MC3T3-E1 did not display intrinsic *Fgf23* expression. Nevertheless, after 2 weeks osteogenic differentiation of MC3T3-E1, *Fgf23* mRNA expression was induced by 10 nM 1,25$(OH)_2$D. 1,25$(OH)_2$D-induced *Fgf23* mRNA expression was completely repressed by hypoxic conditions (0.2% O_2) for 24 or 48 hours and hypoxia alone failed to trigger *Fgf23* expression (Figure S7 a). The upregulation of the HIF-1 target genes carbonic anhydrase 9 (*Car9*) and prolyl hydroxylase domain containing protein 2 (*Phd2*) confirmed the presence of hypoxia (Figure S7 b and c). Similarly, hypoxia had no effect on *Fgf23* mRNA expression in U2OS rat osteosarcoma and primary osteoblast cells (data not shown). We analyzed also kidneys of von Hippel-Lindau (*Vhl*) KO animals [46]. Lack of VHL prevents HIF hydroxylation and degradation and activates hypoxia sensitive genes [47]. Neither the kidneys of *Vhl* KO animals nor primary kidney cells lacking *Vhl* [48] expressed any detectable *Fgf23* (data not shown).

TNF blockade lowers FGF23 levels in mouse models of oxalate nephropathy and colitis

We expanded our observations to another CKD mouse model, the oxalate nephropathy model [49]. After induction of oxalate nephropathy, 48 hours prior to sacrifice, mice received a single i.p. injection of 0.5 mg anti-TNF or isotypic IgG control antibodies. IgG injected oxalate nephropathy mice had elevated plasma iFGF23 compared to control mice and TNF blockade normalized the elevated plasma iFGF23 in oxalate nephropathy mice (Figure 5 a). Plasma cFGF23 and iFGF23/cFGF23 did not differ between the groups

(Figure S4 g – i). Plasma TNF was significantly reduced in the anti-TNF treated groups confirming the efficacy of the anti-TNF antibody (Figure 5 b). There was no difference in plasma TNF between IgG control treated oxalate nephropathy and control mice. Renal *Tnf* mRNA expression showed a clear trend to increase in oxalate nephropathy mice and was not affected by the anti-TNF antibody (Figure 5 c). There was no change in plasma phosphate and urine phosphate per urine creatinine ratio while the renal function parameters plasma creatinine and urea showed a trend to increase in the oxalate nephropathy mice (Figure 5 d – g).

To demonstrate that TNF regulates plasma iFGF23 independent from impaired kidney function, we analyzed a non-renal inflammation model, the *Il10* KO mouse developing spontaneously colitis [50]. Twelve to fourteen weeks old *Il10* KO mice had elevated plasma iFGF23 and increased colon *Tnf* mRNA expression (Figure 6 a and b). After 48 hours of a single i.p. injection of 0.5 mg anti-TNF or IgG control, anti-TNF treated *Il10* KO mice had reduced plasma iFGF23 compared to IgG treated animals whereas cFGF23 levels were similar. There was a reduction in the iFGF23/cFGF23 ratio in anti-TNF treated *Il10* KO compared to IgG control treated *Il10* KO mice (Figure S4 j – l). Anti-TNF treatment had no effect on plasma phosphate levels (Figure 6 c and d) or kidney function parameters (Figure 6 e and f). But there was an increase in abundance of NaPi-IIa at the BBM in *Il10* KO mice treated with anti-TNF antibodies compared to IgG control mice (Figure 6 g)

Discussion

We provide a novel explanation for high iFGF23 levels in patients with chronic kidney disease or inflammation of non-renal origin. Our data demonstrate that TNF is positively and independently associated with plasma iFGF23 in humans. We show that exogenous TNF stimulates iFGF23 expression both *in vivo* and *in vitro*. TNF neutralization suppresses plasma iFGF23 in two CKD mouse models and triggers renal *Fgf23* expression in PKD kidneys. TNF also contributes to high iFGF23 in a model of intestinal inflammation with normal kidney function.

In humans, TNF levels correlated with plasma iFGF23 in the SKIPOGH multi-centric population based cohort. Dhayat et al. found in the same cohort associations between cFGF23 and plasma phosphate, $1,25(OH)_2D$, 25(OH)D, the ratio of TmP/GFR, age, sex, and renal function. However, there are relevant differences between both analyses: 1) we have measured the biologically active iFGF23 and Dhayat et al. [51] used a method that detects both the intact form and the biologically inactive C-terminal fragment. 2) in addition to the subjects excluded by Dhayat et al. we excluded individuals taking drugs interacting with inflammation and subjects without complete data available for all variables. However, both analyses identified $1,25(OH)_2D$ and 25(OH)D as strong predictors of FGF23 variation in the SKIPOGH population while the correlation of PTH and eGFR in our study was dependent on drug exclusion criteria.

TNF increases in kidney disease and associates with CKD progression [14, 31, 32]. TNF stimulates *Fgf23* mRNA expression in an osteocyte-derived cell line [22] and may be involved in obesity induced increases in FGF23 [26]. We tested the relevance of FGF23 regulation by TNF in pathological situations such as kidney disease or colitis. We used two distinct CKD mouse models, the *Pkd1* conditional KO mouse and the oxalate nephropathy model. PKD kidneys are affected by inflammation [52, 53] as confirmed by higher renal *Tnf* and *Tgfb* expression as well as enhanced NFκB subunit p65 phosphorylation. Similarly, in oxalate nephropathy the inflammasome is activated and

266 various proinflammatory cytokines are released [49, 54]. Ectopic renal FGF23 gene and
267 protein expression occurs in rodents with either diabetic nephropathy, PKD, or 5/6
268 nephrectomy [34, 55, 56]. The increase of renal *Tnf* and *Tgfb* mRNA expression in PKD
269 kidneys was paralleled by the increase in plasma iFGF23 levels, and the appearance of
270 renal *Fgf23* and *Runx-2* expression. Renal FGF23 production may promote inflammation
271 and fibrosis in the affected kidney [35, 36, 57]. We did not detect any change in bone *Fgf23*
272 mRNA expression or plasma TNF levels in both CKD models. Similarly, in *Col4a3* KO
273 mice, another CKD model, the early rise in plasma FGF23 is not accompanied by
274 increased *Fgf23* expression in bone [58]. TNF blockade in both CKD models normalized
275 plasma iFGF23 levels without changes in plasma phosphate levels. In the PKD model,
276 TNF neutralization also reduced renal *Fgf23* expression. TNF may regulate renal *Fgf23*
277 expression through NFκB stimulating orphan nuclear receptor *Nurr1* gene expression [38].
278 Nurr1 mediates the PTH dependent regulation of *Fgf23* in bone [37]. *Nurr1* was upregulated
279 in PKD kidneys and predominantly localized in the cell nucleus whereas in wild type
280 kidneys it was localized in the cytoplasm. Nurr1 nuclear localization often overlapped with
281 renal FGF23 protein expression. Thus, Nurr1 may contribute to renal FGF23 expression.

282 In patients with CKD, TNF increases with ascending FGF23 quartiles and correlates with
283 FGF23 levels independent of renal function and measures of mineral metabolism [14].
284 Likewise, markers of inflammation correlate with ascending FGF23 quartiles in non-CKD
285 stroke patients [16]. Inoculation of mice with LPS or bacteria stimulates serum FGF23 levels
286 [23, 27]. In the diabetic nephropathy rat model, renal FGF23 was reduced by ramipril, an
287 angiotensin-converting enzyme inhibitor [56], which also reduces inflammation [59]. Non-
288 renal diseases characterized by inflammation such as inflammatory bowel disease (IBD)
289 or osteoarthritis are linked to elevated plasma FGF23 [17, 18]. Patients with IBD or mouse
290 colitis models show elevated FGF23 levels, lower 1,25$(OH)_2$D and impaired intestinal
291 phosphate absorption [17, 60-63]. These disturbances are partially caused by TNF and in
292 patients with IBD, TNF neutralizing therapy can reverse some of these abnormalities. We
293 tested whether inflammation *per se* without renal disease could increase FGF23.

294 Consistently, in *Il-10* KO mice, a model of IBD, plasma FGF23 increased and was
295 reduced by TNF neutralization without affecting renal function parameters. Thus,
296 extrarenal inflammation also stimulates FGF23 levels in mouse models and may play a
297 role in humans.

298 David et al. reported that 6 hours after administration of the inflammatory cytokine IL-1β
299 only cFGF23 increased while it required 4 days of consecutive IL-1β injections to
300 increase also iFGF23 levels [24], whereas Onal et al showed higher FGF23 levels already
301 3 hours after IL-1β injection [27]. We demonstrate that TNF administration in wild type mice
302 stimulated plasma iFGF23 levels within 48 hours without altering plasma phosphate and
303 creatinine but increasing fractional excretion of phosphate demonstrating that iFGF23 is
304 functional. TNF may exert even faster effects as indicated by higher FGF23 levels in mice
305 3 hours after TNF injection [27]. The stimulation of *Fgf23* mRNA expression by TNF was
306 confirmed *in vitro* in primary mouse osteocytes and comparable to the effect of
307 $1,25(OH)_2D$. TNF but not $1,25(OH)_2D$ increased *Nurr1* and *Galnt3* expression in primary
308 osteocytes suggesting that TNF but not $1,25(OH)_2D$ may regulate *Fgf23* expression in a
309 Nurr1-dependent manner. TNF may also modulate FGF23 protein stability by regulating
310 the expression of *Galnt3* which mediates the O-glycosylation of FGF23 making it more
311 resistant to proteolytic degradation [43]. In bone, C-terminal DMP-1 binds to PHEX and
312 thereby inhibits *Fgf23* expression [64]. In primary osteocytes, *Dmp1* expression was
313 strongly decreased by TNF and $1,25(OH)_2D$. The upregulation of *Fgf23* expression by
314 TNF and $1,25(OH)_2D$ is paralleled by the downregulation of its suppressor. Our data
315 expand previous observations in IDG-SW3 mouse osteocyte cells where TNF, IL-1β, and
316 LPS increased *Fgf23* and reduced *Dmp1* mRNA expression [22]. TNF also stimulated
317 *Fgf23* mRNA expression in rat UMR106 osteosarcoma cells and is required to increase
318 circulating FGF23 levels in a mouse obesity model [25]. Deletion of an 16kb enhancer
319 element in the *Fgf23* murine gene abolishes TNF induced FGF23 increases and reduces
320 the effect of LPS and IL-1β on circulating FGF23 levels without altering bone structure or
321 plasma phosphate and PTH. Induction of *Fgf23* mRNA in various organs is organ-

specifically responsive to LPS, TNF and IL-1β and the deletion of the enhancer suggesting a complex and cell- and/or organ-specific regulation [27]. The enhancer element is also required for the early induction of FGF23 in the oxalate nephropathy model [27]. Thus, our work demonstrates the critical role of TNF in inducing FGF23 production and thereby complements previous work that identified a genetic element responding to TNF and possibly other regulators of *Fgf23* mRNA transcription [27]. Furthermore, we expand these observations from kidney disease to at least one other clinically important condition, inflammatory bowel disease.

IL-6 has been recently identified as another important proinflammatory cytokine that associates with FGF23 levels in the CRIC cohort [14] and that stimulates *Fgf23* mRNA in the IDG-SW3 osteocyte cell line [22]. Durlacher-Betzer et al. showed increased expression of IL-6 in kidney of folic-acid and adenine AKI and CKD mouse models and a partly blunted increase of circulating FGF23 levels in Il-6 deficient mice treated with adenine [28]. While IL-6 may participate in the regulation of FGF23 in CKD, IL-6 plays also an important role in normal bone biology and IL-6 deficient mice have altered bone architecture [65, 66]. Thus, IL-6 may contribute to the upregulation of FGF23 in early CKD but TNF may act either upstream or is a critical permissive factor as indicated by the complete normalization of FGF23 levels in our experiments. In our population-based cohort, TNF but not IL-6 associated with intact FGF23 levels further strengthening the concept that TNF may play a central role in mediating effects of inflammation on bone.

Renal hypoxia is a common complication in CKD kidneys [44, 45]. Hypoxia increased *Fgf23* expression in UMR-106 rat osteosarcoma cells, and plasma cFGF23 but not iFGF23 in rats under hypobaric hypoxia conditions [21]. We cultured MC3T3-E1 cells, a mouse preosteoblast cell line and primary mouse osteoblasts for 24 and 48 hours in 0.2% hypoxia and we did not observe any stimulation of *Fgf23* expression. In contrast, hypoxia suppressed the stimulatory effect of $1,25(OH)_2D$ on *Fgf23*. TNF and IL-1β increase HIF-1 binding to DNA under normoxia while in combination with hypoxia both cytokines

349 strongly increase HIF-1 activity [67]. IL-1β but not TNF enhance nuclear accumulation of
350 HIF-1α in a hepatoma cell line [67] and increase FGF23 mRNA expression in bones and
351 kidneys [24]. Inhibition of HIF-1α attenuated the positive effect of IL-1β on FGF23
352 expression [24]. Combined with the fact that we did not find any effect of constitutively
353 activated HIF-1α in *Vhl* KO animals as well as in primary kidney cells lacking *Vhl*, these
354 results suggest that the HIF-1α mediated upregulation of *Fgf23* expression may depend
355 on IL-1β or other factors such as erythropoietin [11, 24, 68, 69].

356 In summary, TNF stimulates iFGF23 in renal and non-renal inflammatory mouse models
357 and in primary bone cell culture; triggers renal *Fgf23* expression in CKD animal models
358 and is positively associated with plasma iFGF23 in a population-based cohort. These
359 findings question the concept that the early rise in plasma FGF23 in CKD is solely to
360 balance plasma phosphate while kidney function declines or if other non-renal processes
361 may strongly impact on plasma FGF23 levels. Our study suggests novel therapeutic
362 options to reduce excessive FGF23 levels in kidney and other diseases as drugs lowering
363 TNF are widely clinically used and have proven to be safe in humans.

364

Methods

SKIPOGH cohort

We obtained 1098 out of 1131 human EDTA plasma samples from SKIPOGH cohort (Swiss Kidney Project on Genes in Hypertension) [29, 70, 71]. Plasma iFGF23 was measured with the human intact FGF23 ELISA kit (Immutopics International, USA). For statistical modeling the following 18 previously determined parameters were used: plasma calcium, phosphate, ferritin, transferrin, iron, $1,25(OH)_2D$, 25(OH) vitamin D_3, PTH, TNF, IFNγ, IL-1β, IL-6, IL-10 and cFGF23 as well as body mass index, age, sex and estimated renal function calculated by the CKD-EPI equation.

Exclusion criteria followed the pipeline described in the Table S3. Participants with incomplete data sets (n = 261) were excluded. TNF followed a bimodal distribution with 40 values close to undetectable (TNF < 1 pg/ml) without continuity with the rest of the distribution, highly suggestive for measurement failures. Therefore the 40 participants with TNF < 1 pg/ml were excluded from the study. Next, the ratio between iFGF23 (detects only iFGF23) and cFGF23 (detects iFGF23 and cFGF23) was calculated. One Ru/ml cFGF23 corresponds to 1.5 pg/ml iFGF23 (information provided by Immutopics); participants with ratios higher than 1.5 were excluded (n = 40). To avoid confounding effects by drug intake we eliminated 4 major drug categories that interact with FGF23 metabolism: 1) calcium, phosphate and magnesium (n = 41); 2) inflammation (pro or anti-inflammatory) (n = 390); 3) iron metabolism (n = 6); 4) kidney function (i.e. diuretics) (n = 54) (Table S4). A total of 361 participants were excluded due to intake of drugs of one or more of these drug categories. The final dataset contains either 429 participants (198 female / 231 male) with or 790 (424 female / 366 male) without drug exclusion criteria.

Animals

Pkd1 floxed/floxed (*$Pkd1^{fl/fl}$*) tamoxifen inducible *cre* mice were kindly provided by Gregory Germino [33, 72]. *Cre* recombinase expression is under the control of the β-actin promoter which drives high levels of expression in most tissues [33]. Male and female

392 *Pkd1*$^{fl/fl}$*, cre+* and *Pkd1*$^{fl/fl}$*, cre-* mice were used. Cre recombinase activity was induced at
393 postnatal days 15, 17, and 19 by injecting pups with 100 µl tamoxifen (2.5 mg/ml) in corn
394 oil causing slow onset disease [33]. Without further interventions, 24-hour urine was
395 collected from 6 and 12 weeks old animals (e.g. 3 or 9 weeks after induction, respectively)
396 which were thereafter sacrificed to collect plasma and organs. For TNF blockade, animals
397 were treated at the age of 11-12 weeks with a single i.p. injection of 0.5 mg *InVivo*MAb
398 anti-Tnfα (Clone XT3.11, Lot4653-1/0413, BioXCell, USA) or *InVivo*MAb rat IgG1 (Clone
399 HRPN, Lot 5339/1014, BioXCell, USA) [73, 74]. Twenty-four hours after antibody application,
400 animals were sacrificed and plasma and organs were collected. The effect of TNF in wild-
401 type mice was assessed by injecting 13 weeks old C57Bl/6J mice on two consecutive
402 days with 2 µg TNF. After 48 hours, plasma and organs were collected.
403 Nephropathy was induced in 10 to 12 weeks old C57Bl/6J mice. After 3 days of
404 adaptation with calcium-free diet (irradiated S7042-E005S, Sniff Spezialdiäten GmbH,
405 Germany), mice were fed for 10 days with either calcium free diet or 0.67% oxalate in
406 calcium-free diet (irradiated S7042-E010) followed by a 5-day recovery phase in standard
407 diet (3433, Kliba, Kaiseraugst, Switzerland). Forty-eight hours prior to sacrifice, mice
408 received a single i.p. injection of 0.5 mg anti-TNF or isotypic IgG1 control. Mice were
409 sacrificed and plasma and organs were collected.
410 *Il10* deficient mice (*Il10*$^{-/-}$) develop spontaneous colitis and were used as a non-renal
411 inflammatory disease model [50]. *Il10*$^{-/-}$ mice between 12-14 weeks were sacrificed to
412 collect plasma and organs. *Il10*$^{-/-}$ mice were treated with a single i.p. injection of 0.5 mg
413 *InVivo*MAb anti-Tnfα (Clone XT3.11, Lot4653-1/0413, BioXCell, USA) or *InVivo*MAb rat
414 IgG1 (Clone HRPN, Lot 5339/1014, BioXCell, USA) [73, 74] 48 hours prior to sacrifice and
415 plasma and organs were collected. For some experiments, kidneys from kidney-specific
416 von-Hippel-Lindau deficient mice were used [46]. All animal studies were performed
417 according to protocols approved by the legal authority (Veterinary Office of the Canton
418 of Zurich or the Committee on Animal Research, University of California San Francisco).

Plasma and urine analysis

Blood and 24 hours urine were collected from *Pkd1*$^{fl/fl}$*, cre+* and *Pkd1*$^{fl/fl}$*, cre-* mice at 6 and 12 weeks after birth. Briefly, *Pkd1*$^{fl/fl}$*, cre* mice were kept for three days in metabolic cages (Tecniplast, Italy) whereas the last day was used for 24 hours urine collection. Afterwards mice were anesthetized with isoflurane and blood was collected from the heart. Plasma and urine aliquots were rapidly frozen and stored at -80 °C until measurement. Urine and plasma laboratory analyses were performed on a UniCel DxC 800 Synchron (Beckman Coulter, Switzerland) by the Zurich Integrative Rodent Physiology (ZIRP) core facility. The ratio of the maximum rate of tubular phosphate reabsorption to the glomerular filtration rate (TmP/GFR) was calculated as follows: $TmP/GFR\ in\ mmol/L = P_P - [U_P \times P_{crea} / U_{crea}]$ where P_P, U_P, P_{crea}, and U_{crea} refer to the plasma and urinary concentration of phosphate and creatinine, respectively [75]. The plasma concentration of intact FGF23 (Kainos Laboratories, Japan or Immutopics International, USA), intact PTH (Immutopics International, USA) and TNF (Bio-Techne AG, Switzerland) were measured by enzyme-linked immunosorbent assays according to the manufacturers protocols.

Cell culture

All cell culture reagents were from Life Technologies Europe B.V. (Switzerland) unless stated otherwise. Two to four month old *Pkd1*$^{fl/fl}$*, cre* mice (4-6 mice per experiment, male and female mixed) were sacrificed with carbon dioxide. Tibias and femurs from the hindlegs were harvested. The epiphyses were cut and bones were flushed with Hank's Balanced Salt Solution (HBSS) containing 1% penicillin streptomycin (Pen Strep) to remove the bone marrow. Bones were cut into small pieces of 1-2 mm^2. Bone cell extraction was performed according to established protocols [39, 40]. Briefly, small bone pieces were repeatedly digested with either a solution containing 2 mg/ml collagenase type II, 0.05% (w/v) soybean trypsin inhibitor (Sigma-Aldrich, Switzerland), 20 mM HEPES, 1% Pen Strep in HBSS or 10 nM EDTA, 1% fetal bovine serum (FBS), 1% Pen

Strep in phosphate buffered saline (PBS) for 25 min at 37°C. Cells from digestion steps 6-9 or cells and bone pieces from digestion step >9 were cultured for 2 weeks in an osteogenic medium (minimal essential medium α (memα) containing 10% FBS, 1% Pen Strep, 50 µg/ml 2-phospho-L-ascorbic acid trisodium salt (Sigma-Aldrich, Switzerland), and 1 mM β-glycerophosphate (Sigma-Aldrich, Switzerland)). After 2 weeks, cells were supplemented for 24 hours with either 10 nM $1,25(OH)_2D$ (CaymanChemical, USA) or 10 ng/ml mouse TNF (R&D Systems, USA) and total mRNA was extracted.

MC3T3-E1 subclone 4 preostoblast cells (CRL-2593, Lot 59899932, ATCC France) passage 17/4 were expanded for 4-5 days with MEMα medium supplemented with 10% FBS and 1% PenStrep. After reaching 80-90% confluence, MC3T3-E1 cells were trypsinized and plated in collagen coated 6-well plates (80'000 cells/well). Medium was changed to osteogenic differentiation medium (MEMα supplemented with 10% FBS, 1% PenStrep, 50µg/ml 2-phospho-L-ascorbic acid trisodium salt (Sigma-Aldrich, Switzerland), and 1 mM beta glycerophosphate (Sigma-Aldrich, Switzerland)). After 2 weeks differentiation along the osteogenic lineage cells were supplemented for 24 or 48 hours with either 10 nM $1,25(OH)_2D$ (CaymanChemical, USA) or an equal amount of ethanol and incubated for 24 or 48 hours under hypoxic (0.2% O_2) or normoxic conditions. Hypoxia experiments were performed in a gas-controlled workstation (InvivoO_2, Baker Ruskinn, UK).

RNA extraction, reverse transcription and qPCR

Organs and scraped colonic mucosa were harvested and rapidly frozen in liquid nitrogen. Tissues were homogenized using either a Precellys homogenizer or a liquid nitrogen cooled mortar and pestle (bone). Total mRNA from bone as well as from cultured cells was extracted with TRIzol (Life Technologies Europe B.V., Switzerland) followed by purification with RNeasy Mini Kit (Qiagen, Switzerland) according to the manufacturers protocol. Total mRNA from kidney and colonic mucosa were extracted with RNeasy Mini Kit (Qiagen, Switzerland) according to the manufacturer's protocol. DNAse digestion was performed using the RNase-free DNAase Set (Qiagen, Switzerland). Total RNA

extractions were analyzed for purity and concentration using the NanoDrop ND-1000 spectrophotometer (Wilmington, Germany). RNA samples were diluted to a final concentration of 100 ng/µl and cDNA was prepared using the TaqMan Reverse Transcriptase Reagent Kit (Applied Biosystems, Roche, Foster City, CA). In brief, in a reaction volume of 40 µl, 300 ng of RNA was used as template and mixed with the following final concentrations of RT buffer (1x): $MgCl_2$ (5.5 mmol/l), random hexamers (2.5 µmol/l), dNTP mix (500 µmol/l each), RNase inhibitor (0.4 U/µl), multiscribe reverse transcriptase (1.25 U/µl), and RNAse-free water. Reverse transcription was performed with temperature conditions set at 25˚C for 10 min, 48˚C for 30 min, and 95˚C for 5 min on a thermocycler (Biometra, Germany). Quantitative PCR (qPCR) was performed on the ABI PRISM 7700 Sequence Detection System (Applied Biosystems). Primers for genes of interest were designed using Primer 3 software. Primers were chosen to span exon - exon boundaries to exclude the amplification of contaminating genomic DNA (primer and probe sequence see Table S5). The specificity of all primers was tested and always resulted in a single product of the expected size (data not shown). Probes were labeled with the reporter dye FAM at the 5'-end and the quencher dye TAMRA at the 3'-end (Microsynth, Switzerland). qPCR reactions were performed using the KAPA PROBE FAST qPCR Kit (KappaBiosystems, USA) or PowerUp™ SYBR® Green Master Mix (Applied Biosystems, Switzerland).

Protein extraction and Western blot analysis

Organs were rapidly frozen in liquid nitrogen. Tissues were homogenized in homogenization buffer containing 0.27 M sucrose, 2 mM EDTA (pH8), 0.5% NP-40, 60 mM KCl, 15 mM NaCl, 15 mM HEPES (pH7.5) (all Sigma-Aldrich, Switzerland) and complete protease inhibitor cocktail (Roche, Switzerland) using Precellys homogenizer. Nuclei were separated by a sucrose cushion and resuspended in a nuclear extraction buffer containing 20 mM HEPES (pH 7.5), 400 mM NaCl, 1 mM EDTA (pH 8), 1 mM DTT and 1 mM PMSF (all Sigma-Aldrich, Switzerland). After measurement of protein concentration (Bio-Rad, Hercules, CA, USA), 60 µg of nuclear proteins were solubilized

in loading buffer containing DTT and separated on a 10% polyacrylamide gel. For immunoblotting, proteins were transferred electrophoretically to polyvinylidene fluoride membranes (Immobilon-P, Millipore, Bedford, MA, USA). After blocking with 5% milk powder in Tris-buffered saline/0.1% Tween-20 or 5% bovine serum albumin (BSA) in Tris-buffered saline/0.1% Tween-20 for 60 min, blots were incubated with the primary antibodies: mouse monoclonal anti-phospho-NFκB p65 (Ser536)(7F1) (Cell Signaling Technology, USA; 1:1000) or rabbit monoclonal NFκB p65 (D14E12) (Cell Signaling Technology, USA; 1:1000) either for 2 h at room temperature or overnight at 4˚C. Membranes were then incubated for 1 h at room temperature with secondary goat anti-rabbit or donkey anti-mouse antibodies (1:5000) linked to alkaline phosphatase (Promega, USA) or HRP (Amersham, MA, USA or R&D Systems, USA). The protein signal was detected with the appropriate substrates using the DIANA III-chemiluminescence detection system (Raytest, Straubenhardt, Germany). All images were analyzed using the software Advanced Image Data Analyser AIDA, Raytest to calculate the ratio between phosphorylated protein to total protein.

Immunofluorescence staining

Mouse kidneys were perfused through the left heart ventricle with a fixative solution containing 3% paraformaldehyde in phosphate buffered saline (PBS). Kidneys were embedded in TissueTec and frozen in liquid nitrogen. Five µm cryosections were cut. Slides were rehydrated with PBS, treated for 5 min with 0.5% SDS in PBS followed by 10 min treatment with 0.5% Triton-X-100 in PBS (Sigma-Aldrich, Switzerland). Unspecific sites were blocked with 1% bovine serum albumin (BSA) in PBS for 1 h at room temperature. Primary antibodies were diluted in 1% BSA in PBS (rat anti-FGF23 clone #283507 (R&D Systems, USA) 1:1000; rabbit anti-Nurr1 N-20 sc-991 (Santa-Cruz, USA) 1:200) and kidney sections were incubated with the primary antibody overnight at 4˚C. After washing with PBS, sections were incubated with the corresponding secondary antibody (1:500) (anti-rabbit DyLight 594 (Jackson ImmunoResearch, Europe), anti-rat NL493 (R&D Systems, USA)), and DAPI (Life Technologies Europe B.V., Switzerland,

1:1000) for 1 h at room temperature. Slides were washed twice with PBS before they were mounted with Dako glycergel mounting medium (Dako, Switzerland). Sections were visualized on a Leica DM 5500B fluorescence microscope and images processed with ImageJ.

Statistical analysis

Statistics were performed using unpaired Student's t-test, ANOVA, or Two-Way-ANOVA (GraphPad Prism version 7, GraphPad, San Diego, CA) and R programming environment including the nlme, visreg, data.table, car, lmtest, and forestplot packages. $P < 0.05$ was considered significant.

The identification of predictors for iFGF23 variation in the SKIPOGH population was performed using linear mixed models with random intercept. The distribution of all parameters was analyzed in histograms. Due to a heavily skewed distribution, IL-6, IL-10, IFNγ and IL1-β were log-transformed. All parameters were centralized and then normalized by their standard deviations. Linear or nonlinear relationship of each variable with iFGF23 was assessed using a component residual plot. However, all parameters were considered linear. Assumptions on the within-group error were checked with plots of the standardized residuals versus fitted values and a Q-Q plot of the residuals. The assumptions on the random effects were checked with a Q-Q plot of the random effects.

Author contributions

Conceptualization, D. E-S., P.H.I.S., and C.A.W; Methodology, D. E-S., P.H.I.S., and C.A.W; Formal analysis, D. E-S. and P.H.I.S.; Investigation, D. E-S., P.H.I.S., B.G., N.G., C.B., M.Z., D.S., M.R., D.A., B.P., M.P., A.L., and G.-M. F; Resources C.A.W., D.H., F.K., I.F-W., G.R., M. B., F.P., M.F., F.L., R.H.W. and I.F.; Writing – Original Draft, D. E-S. Writing -Review & Editing, D. E-S., P.H.I.S., and C.A.W; Visualization, D. E-S. and P.H.I.S.; Supervision, C.A.W.; Funding Acquisition, C.A.W, all authors read, edited and approved the manuscript.

Acknowledgments

This study was supported by grants from the Swiss National Center for Competence in Research NCCR Kidney.CH to C. A. Wagner, the Novartis Foundation for medical-biological research to C. A. Wagner and D. Egli-Spichtig, the SNSF early postdoc mobility grant to D. Egli-Spichtig and the Deutsche Forschungsgemeinschaft to Michael Föller and Florian Lang (La315-15). P.H. Imenez Silva was recipient of a fellowship from the IKPP Kidney.CH under the European Union Seventh Framework Programme for Research, Technological Development and Demonstration under the grant agreement no 608847 and Conselho Nacional de Desenvolvimento Científico e Tecnológico (CNPq) grant number 205625/2014-2. The use of the ZIRP Core facility for Rodent Physiology is gratefully acknowledged. SKIPOGH was supported by a SPUM grant from the Swiss National Center for Competence in Research (FN 33CM30-124087) and by intramural support of Lausanne, Geneva, and Bern University Hospitals. cFGF23, PTH and vitamin D measurements were supported by an unrestricted research grant from Abbvie (Daniel Fuster and Nasser Dhayat) and by intramural support of Bern University Hospital. We thank the study nurses Marie-Odile Levy, Guler Gök-Sogüt, Ulla Schüpbach, and Dominique Siminski for their involvement and help with recruitment. We also thank Sandrine Estoppey for her help in logistic and database management. SKIPOGH investigators include Murielle Bochud (PI), Fred Paccaud and Michel Burnier, Lausanne University Hospital, Lausanne; Pierre-Yves Martin and Antoinette Péchère-Bertschi, Geneva University Hospitals, Geneva; Bruno Vogt, Inselspital, Bern and Olivier Devuyst, University of Zürich, Zürich. SNFR-supported SKIPOGH-1 fellows include Daniel Ackermann (Inselspital, Bern), Georg Ehret, Idris Guessous and Belen Ponte (Geneva University Hospitals, Geneva) and Menno Pruijm (Lausanne University Hospital, Lausanne).

Conflict of interests

C.A. Wagner has been a member of an advisory board to Bayer Pharma AG, and provided consultancy to Medice. No other financial interests are reported.

Figure legends

Figure 1

Identification of plasma iFGF23 predictors in a human cohort. (a) Forest plot showing the fixed effects calculated for all predictors used in the mixed linear model for the subpopulation of 429 participants after all the exclusion criteria applied. Fixed effect estimates (β), standard error, ratio between the estimates and their standard errors (t-value), and associated p-value from a t-distribution. The parameters are ordered by fixed effect estimates. (b) Association between plasma TNF and iFGF23 in the SKIPOGH cohort in a subpopulation of 429 participants after all the exclusion criteria applied. The regression line and confidence band were obtained from the linear mixed model containing all the predictors.

Figure 2

FGF23 and inflammation in *Pkd1* KO mice. Plasma FGF23 (a) and TmP/GFR (b) as well as renal *Tnf* (e) and renal *Tgfb* (f) mRNA expression relative to 18SrRNA in $Pkd1^{fl/fl}$, *cre-* (white squares) and $Pkd1^{fl/fl}$, *cre+* (black squares) animals after 6 and 12 weeks. Phosphorylation of NFκB p65 (g) in the nuclear fraction of total kidney protein homogenates in $Pkd1^{fl/fl}$, *cre-* (white squares) and $Pkd1^{fl/fl}$, *cre+* (black squares) animals after 12 weeks. Renal (f) and bone (g) *Fgf23* mRNA expression relative to 18SrRNA in $Pkd1^{fl/fl}$, *cre-* (white squares) and $Pkd1^{fl/fl}$, *cre+* (black squares) animals after 12 weeks. ND = not detected. Two-way ANOVA with Bonferroni correction (a - d) or unpaired t-test (e - g), * $p<0.05$.

Figure 3

TNF neutralization lowers FGF23 in *Pkd1* KO mice. Plasma TNF (a), iFGF23 (b), phosphate (c), and urea (d) levels, bone (e) and renal (f) *Fgf23*, renal *Tnf* (g), and renal *Tgfb* (h) mRNA expression relative to *Hprt* as well as abundance of NaPi-IIa (i) at the renal BBM relative to β-actin 24 hours after injection of 0.5mg isotypic IgG control or anti-TNF neutralizing antibodies in 11-12 weeks old $Pkd1^{fl/fl}$, *cre-* (white squares) and $Pkd1^{fl/fl}$, *cre+* (black squares) animals. ND = not detected. Two-way ANOVA with Bonferroni correction * $p<0.05$.

Figure 4

TNF stimulates FGF23 *in vivo* and *in vitro*. Plasma iFGF23 (a), TNF (b), phosphate (c), creatinine (d), urea (e) and FEP (f) as well as bone (g), spleen (h) thymus (i) and bone marrow Fgf23 mRNA expression relative to *Hprt* (g,h) or *18SrRNA* (i,j) 48 hours after two consecutive injection of vehicle or 2 µg recombinant mouse TNF in 12 weeks old wild type mice. Unpaired t-test * $p<0.05$. Fold increase of *Fgf23* (k), *Dmp1* (l), *Galnt3* (m), and *Nurr1* (n) mRNA expression compared to untreated control in primary murine osteocytes after stimulation with $1,25(OH)_2D$ (white squares) or 10ng/ml TNF (black squares) for 24 hours. Single experiments were normalized to their untreated control (dashed line = 1). Number of independent experiments 9-10; One-way ANOVA with Bonferroni correction * $p<0.05$ compared to $1,25(OH)_2D$ treated cells, # $p<0.05$ compared to untreated cells.

628 **Figure 5**

629 **TNF neutralization lowers plasma iFGF23 in mice with oxalate nephropathy.**
630 Oxalate-nephropathy was induced in wild type mice. Plasma iFGF23 (a), plasma TNF
631 (b), renal *Tnf* (c) mRNA expression relative to *Hprt*, plasma phosphate (d), urinary
632 phosphate to creatinine ratio (e), plasma creatinine (f) and plasma urea (g) 48 hours after
633 injection of 0.5 mg isotypic IgG control or anti-TNF neutralizing antibodies in control diet
634 (white squares) and oxalate nephropathy (black squares) induced mice. One-way
635 ANOVA with Bonferroni correction * $p<0.05$.

636 **Figure 6**

637 **Colonic inflammation increases plasma iFGF23 via TNF in *Il-10* KO mice.** Plasma
638 iFGF23 (a) levels and colonic *Tnf* (b) mRNA expression relative to 18SrRNA in 14 weeks
639 old *Il-10*$^{+/+}$ and *Il-10*$^{-/-}$ mice. Plasma iFGF23 (c), phosphate (d), creatinine (e), and urea
640 (f) levels as well as abundance of NaPi-IIa at the renal BBM 48 hours after injection of
641 0.5 mg isotypic IgG control or anti-TNF neutralizing antibodies in 12 weeks old *Il-10*$^{-/-}$
642 mice. Unpaired t-test * $p<0.05$.

643

REFERENCES

1. Isakova T, Wahl P, Vargas GS*, et al.* Fibroblast growth factor 23 is elevated before parathyroid hormone and phosphate in chronic kidney disease. *Kidney Int* 2011; **79:** 1370-1378.

2. Block GA, Klassen PS, Lazarus JM*, et al.* Mineral metabolism, mortality, and morbidity in maintenance hemodialysis. *J Am Soc Nephrol* 2004; **15:** 2208-2218.

3. Gutierrez OM. Fibroblast growth factor 23 and disordered vitamin D metabolism in chronic kidney disease: updating the "trade-off" hypothesis. *Clin J Am Soc Nephrol* 2010; **5:** 1710-1716.

4. Gutierrez OM, Mannstadt M, Isakova T*, et al.* Fibroblast growth factor 23 and mortality among patients undergoing hemodialysis. *N Engl J Med* 2008; **359:** 584-592.

5. Faul C, Amaral AP, Oskouei B*, et al.* FGF23 induces left ventricular hypertrophy. *J Clin Invest* 2011; **121:** 4393-4408.

6. Souma N, Isakova T, Lipiszko D*, et al.* Fibroblast Growth Factor 23 and Cause-Specific Mortality in the General Population: The Northern Manhattan Study. *J Clin Endocrinol Metab* 2016; **101:** 3779-3786.

7. Quarles LD. Skeletal secretion of FGF-23 regulates phosphate and vitamin D metabolism. *Nat Rev Endocrinol* 2012; **8:** 276-286.

8. Hu MC, Shiizaki K, Kuro-o M*, et al.* Fibroblast growth factor 23 and Klotho: physiology and pathophysiology of an endocrine network of mineral metabolism. *Annu Rev Physiol* 2013; **75:** 503-533.

9. Urakawa I, Yamazaki Y, Shimada T*, et al.* Klotho converts canonical FGF receptor into a specific receptor for FGF23. *Nature* 2006; **444:** 770-774.

10. Zhang B, Umbach AT, Chen H*, et al.* Up-regulation of FGF23 release by aldosterone. *Biochem Biophys Res Commun* 2016; **470:** 384-390.

11. Daryadel A, Bettoni C, Haider T*, et al.* Erythropoietin stimulates Fibroblast Growth Factor 23 (FGF23) in mice and men. *Pflügers Arch* 2018**:** in press.

12. Bar L, Feger M, Fajol A*, et al.* Insulin suppresses the production of fibroblast growth factor 23 (FGF23). *Proc Natl Acad Sci U S A* 2018; **115:** 5804-5809.

13. Kuro OM, Moe OW. FGF23-alphaKlotho as a paradigm for a kidney-bone network. *Bone* 2017; **100:** 4-18.

14. Mendoza JM, Isakova T, Ricardo AC*, et al.* Fibroblast Growth Factor 23 and Inflammation in CKD. *Clin J Am Soc Nephrol* 2012; **7:** 1155-1162.

15. Wallquist C, Mansouri L, Norrback M*, et al.* Associations of Fibroblast Growth Factor 23 with Markers of Inflammation and Leukocyte Transmigration in Chronic Kidney Disease. *Nephron* 2018; **138:** 287-295.

16. Hanks LJ, Casazza K, Judd SE*, et al.* Associations of fibroblast growth factor-23 with markers of inflammation, insulin resistance and obesity in adults. *PLoS One* 2015; **10:** e0122885.

17. El-Hodhod MA, Hamdy AM, Abbas AA*, et al.* Fibroblast growth factor 23 contributes to diminished bone mineral density in childhood inflammatory bowel disease. *BMC Gastroenterol* 2012; **12:** 44.

18. Iliopoulos D, Malizos KN, Oikonomou P*, et al.* Integrative microRNA and proteomic approaches identify novel osteoarthritis genes and their collaborative metabolic and inflammatory networks. *PLoS One* 2008; **3:** e3740.

19. Dai B, David V, Martin A*, et al.* A comparative transcriptome analysis identifying FGF23 regulated genes in the kidney of a mouse CKD model. *PLoS One* 2012; **7:** e44161.

20. Farrow EG, Davis SI, Summers LJ*, et al.* Initial FGF23-mediated signaling occurs in the distal convoluted tubule. *J Am Soc Nephrol* 2009; **20:** 955-960.

21. Clinkenbeard EL, Farrow EG, Summers LJ*, et al.* Neonatal iron deficiency causes abnormal phosphate metabolism by elevating FGF23 in normal and ADHR mice. *J Bone Miner Res* 2014; **29:** 361-369.

22. Ito N, Wijenayaka AR, Prideaux M*, et al.* Regulation of FGF23 expression in IDG-SW3 osteocytes and human bone by pro-inflammatory stimuli. *Mol Cell Endocrinol* 2015; **399:** 208-218.

23. Masuda Y, Ohta H, Morita Y*, et al.* Expression of Fgf23 in activated dendritic cells and macrophages in response to immunological stimuli in mice. *Biol Pharm Bull* 2015; **38:** 687-693.

24. David V, Martin A, Isakova T*, et al.* Inflammation and functional iron deficiency regulate fibroblast growth factor 23 production. *Kidney Int* 2016; **89:** 135-146.

25. Feger M, Hase P, Zhang B*, et al.* The production of fibroblast growth factor 23 is controlled by TGF-beta2. *Sci Rep* 2017; **7:** 4982.

26. Glosse P, Fajol A, Hirche F*, et al.* A high-fat diet stimulates fibroblast growth factor 23 formation in mice through TNFalpha upregulation. *Nutr Diabetes* 2018; **8:** 36.

27. Onal M, Carlson AH, Thostenson JD*, et al.* A Novel Distal Enhancer Mediates Inflammation-, PTH-, and Early Onset Murine Kidney Disease-Induced Expression of the Mouse Fgf23 Gene. *JBMR Plus* 2018; **2:** 32-47.

28. Durlacher-Betzer K, Hassan A, Levi R*, et al.* Interleukin-6 contributes to the increase in fibroblast growth factor 23 expression in acute and chronic kidney disease. *Kidney Int* 2018.

29. Alwan H, Pruijm M, Ponte B*, et al.* Epidemiology of masked and white-coat hypertension: the family-based SKIPOGH study. *PLoS One* 2014; **9:** e92522.

30. Farrow EG, Yu X, Summers LJ*, et al.* Iron deficiency drives an autosomal dominant hypophosphatemic rickets (ADHR) phenotype in fibroblast growth factor-23 (Fgf23) knock-in mice. *Proc Natl Acad Sci U S A* 2011; **108:** E1146-1155.

31. Amdur RL, Feldman HI, Gupta J*, et al.* Inflammation and Progression of CKD: The CRIC Study. *Clin J Am Soc Nephrol* 2016.

32. Feng YM, Thijs L, Zhang ZY*, et al.* Glomerular function in relation to circulating adhesion molecules and inflammation markers in a general population. *Nephrol Dial Transplant* 2018; **33:** 426-435.

33. Piontek K, Menezes LF, Garcia-Gonzalez MA*, et al.* A critical developmental switch defines the kinetics of kidney cyst formation after loss of Pkd1. *Nat Med* 2007; **13:** 1490-1495.

34. Mace ML, Gravesen E, Nordholm A*, et al.* Kidney fibroblast growth factor 23 does not contribute to elevation of its circulating levels in uremia. *Kidney Int* 2017.

35. Smith ER, Holt SG, Hewitson TD. FGF23 activates injury-primed renal fibroblasts via FGFR4-dependent signalling and enhancement of TGF-beta autoinduction. *Int J Biochem Cell Biol* 2017; **92:** 63-78.

36. Smith ER, Tan SJ, Holt SG*, et al.* FGF23 is synthesised locally by renal tubules and activates injury-primed fibroblasts. *Sci Rep* 2017; **7:** 3345.

37. Meir T, Durlacher K, Pan Z*, et al.* Parathyroid hormone activates the orphan nuclear receptor Nurr1 to induce FGF23 transcription. *Kidney Int* 2014; **86:** 1106-1115.

38. McEvoy AN, Murphy EA, Ponnio T*, et al.* Activation of nuclear orphan receptor NURR1 transcription by NF-kappa B and cyclic adenosine 5'-monophosphate response element-binding protein in rheumatoid arthritis synovial tissue. *J Immunol* 2002; **168:** 2979-2987.

39. Bakker AD, Klein-Nulend J. Osteoblast isolation from murine calvaria and long bones. *Methods Mol Biol* 2012; **816:** 19-29.

40. Stern AR, Stern MM, Van Dyke ME*, et al.* Isolation and culture of primary osteocytes from the long bones of skeletally mature and aged mice. *Biotechniques* 2012; **52:** 361-373.

41. Feng JQ, Ward LM, Liu S*, et al.* Loss of DMP1 causes rickets and osteomalacia and identifies a role for osteocytes in mineral metabolism. *Nat Genet* 2006; **38:** 1310-1315.

42. Topaz O, Shurman, D L, Bergman, R, Indelman, M, Ratajczak, P, Mizrachi, M, Khamaysi, Z, Behar, D, Petronius, D, Friedman, V, Zelikovic, I, Raimer, S, Metzker, A, Richard, G, Sprecher, E. Mutations in *GALNT3*, encoding a protein involved in O-linked glycosylation, cause familial tumoral calcinosis. *Nat Genet* 2004; **36:** 579-581.

43. Kato K, Jeanneau, C, Tarp, M A, Benet-Pages, A, Lorenz-Depiereux, B, Bennett, E P, Mandel, U, Strom, T M, Clausen H. Polypeptide GalNAc-transferase T3 and familial tumoral calcinosis: secretion of FGF23 requires O-glycosylation. *J Biol Chem* 2006; **281:** 18370-18377.

44. Fine LG, Bandyopadhay D, Norman JT. Is there a common mechanism for the progression of different types of renal diseases other than proteinuria? Towards the unifying theme of chronic hypoxia. *Kidney Int Suppl* 2000; **75:** S22-26.

45. Eckardt KU, Bernhardt WM, Weidemann A*, et al.* Role of hypoxia in the pathogenesis of renal disease. *Kidney Int Suppl* 2005**:** S46-51.

46. Frew IJ, Thoma CR, Georgiev S*, et al.* pVHL and PTEN tumour suppressor proteins cooperatively suppress kidney cyst formation. *EMBO J* 2008; **27:** 1747-1757.

47. Maxwell PH, Wiesener MS, Chang GW*, et al.* The tumour suppressor protein VHL targets hypoxia-inducible factors for oxygen-dependent proteolysis. *Nature* 1999; **399:** 271-275.

48. Schonenberger D, Harlander S, Rajski M*, et al.* Formation of Renal Cysts and Tumors in Vhl/Trp53-Deficient Mice Requires HIF1alpha and HIF2alpha. *Cancer Res* 2016; **76:** 2025-2036.

49. Mulay SR, Eberhard JN, Pfann V*, et al.* Oxalate-induced chronic kidney disease with its uremic and cardiovascular complications in C57BL/6 mice. *Am J Physiol Renal Physiol* 2016**:** ajprenal 00488 02015.

50. Kullberg MC, Rothfuchs AG, Jankovic D*, et al.* Helicobacter hepaticus-induced colitis in interleukin-10-deficient mice: cytokine requirements for the induction and maintenance of intestinal inflammation. *Infect Immun* 2001; **69:** 4232-4241.

51. Dhayat NA, Ackermann D, Pruijm M*, et al.* Fibroblast growth factor 23 and markers of mineral metabolism in individuals with preserved renal function. *Kidney Int* 2016; **90:** 648-657.

52. Zeier M, Fehrenbach P, Geberth S*, et al.* Renal histology in polycystic kidney disease with incipient and advanced renal failure. *Kidney Int* 1992; **42:** 1259-1265.

53. Li X, Magenheimer BS, Xia S*, et al.* A tumor necrosis factor-alpha-mediated pathway promoting autosomal dominant polycystic kidney disease. *Nat Med* 2008; **14:** 863-868.

54. Mulay SR, Anders HJ. Crystallopathies. *N Engl J Med* 2016; **374:** 2465-2476.

55. Spichtig D, Zhang H, Mohebbi N*, et al.* Renal expression of FGF23 and peripheral resistance to elevated FGF23 in rodent models of polycystic kidney disease. *Kidney Int* 2014.

56. Zanchi C, Locatelli M, Benigni A*, et al.* Renal Expression of FGF23 in Progressive Renal Disease of Diabetes and the Effect of Ace Inhibitor. *PLoS One* 2013; **8:** e70775.

57. Zhang X, Guo K, Xia F*, et al.* FGF23(C-tail) improves diabetic nephropathy by attenuating renal fibrosis and inflammation. *BMC Biotechnol* 2018; **18:** 33.

58. Stubbs JR, He N, Idiculla A*, et al.* Longitudinal evaluation of FGF23 changes and mineral metabolism abnormalities in a mouse model of chronic kidney disease. *J Bone Miner Res* 2012; **27:** 38-46.

59. Fernandez M, Triplitt C, Wajcberg E*, et al.* Addition of pioglitazone and ramipril to intensive insulin therapy in type 2 diabetic patients improves vascular dysfunction by different mechanisms. *Diabetes Care* 2008; **31:** 121-127.

60. Liu N, Nguyen L, Chun RF*, et al.* Altered endocrine and autocrine metabolism of vitamin D in a mouse model of gastrointestinal inflammation. *Endocrinology* 2008; **149:** 4799-4808.

61. Chen H, Xu H, Dong J*, et al.* Tumor necrosis factor-alpha impairs intestinal phosphate absorption in colitis. *Am J Physiol Gastrointest Liver Physiol* 2009; **296:** G775-781.

62. Augustine MV, Leonard MB, Thayu M*, et al.* Changes in vitamin D-related mineral metabolism after induction with anti-tumor necrosis factor-alpha therapy in Crohn's disease. *J Clin Endocrinol Metab* 2014; **99:** E991-998.

63. Agrawal M, Arora S, Li J*, et al.* Bone, inflammation, and inflammatory bowel disease. *Curr Osteoporos Rep* 2011; **9:** 251-257.

64. Martin A, David V, Li H*, et al.* Overexpression of the DMP1 C-terminal fragment stimulates FGF23 and exacerbates the hypophosphatemic rickets phenotype in Hyp mice. *Mol Endocrinol* 2012; **26:** 1883-1895.

65. Bellido T, Jilka RL, Boyce BF*, et al.* Regulation of interleukin-6, osteoclastogenesis, and bone mass by androgens. The role of the androgen receptor. *J Clin Invest* 1995; **95:** 2886-2895.

66. Wang C, Tian L, Zhang K*, et al.* Interleukin-6 gene knockout antagonizes high-fat-induced trabecular bone loss. *J Mol Endocrinol* 2016; **57:** 161-170.

67. Hellwig-Burgel T, Rutkowski K, Metzen E*, et al.* Interleukin-1beta and tumor necrosis factor-alpha stimulate DNA binding of hypoxia-inducible factor-1. *Blood* 1999; **94:** 1561-1567.

68. Clinkenbeard EL, Hanudel MR, Stayrook KR*, et al.* Erythropoietin stimulates murine and human fibroblast growth factor-23, revealing novel roles for bone and bone marrow. *Haematologica* 2017; **102:** e427-e430.

69. Flamme I, Ellinghaus P, Urrego D*, et al.* FGF23 expression in rodents is directly induced via erythropoietin after inhibition of hypoxia inducible factor proline hydroxylase. *PLoS One* 2017; **12:** e0186979.

70. Pruijm M, Ponte B, Ackermann D*, et al.* Heritability, determinants and reference values of renal length: a family-based population study. *Eur Radiol* 2013; **23:** 2899-2905.

71. Ponte B, Pruijm M, Ackermann D*, et al.* Reference values and factors associated with renal resistive index in a family-based population study. *Hypertension* 2014; **63:** 136-142.

72. Piontek KB, Huso DL, Grinberg A*, et al.* A functional floxed allele of Pkd1 that can be conditionally inactivated in vivo. *J Am Soc Nephrol* 2004; **15:** 3035-3043.

73. Grinberg-Bleyer Y, Saadoun D, Baeyens A*, et al.* Pathogenic T cells have a paradoxical protective effect in murine autoimmune diabetes by boosting Tregs. *J Clin Invest* 2010; **120:** 4558-4568.

74. Carlson MJ, West ML, Coghill JM*, et al.* In vitro-differentiated TH17 cells mediate lethal acute graft-versus-host disease with severe cutaneous and pulmonary pathologic manifestations. *Blood* 2009; **113:** 1365-1374.

75. Brodehl J, Krause A, Hoyer PF. Assessment of maximal tubular phosphate reabsorption: comparison of direct measurement with the nomogram of Bijvoet. *Pediatr Nephrol* 1988; **2:** 183-189.

Figure 1

a

With exclusion by drug intake

	β	SE	t-value	p-value
Intercept	0.029	0.072	0.394	0.694
25(OH)D	0.218	0.054	4.047	<0.001
TNF	0.123	0.059	2.110	0.036
Calcium	0.102	0.049	2.088	0.038
Iron	0.093	0.051	1.819	0.070
IL-6	0.062	0.058	1.072	0.285
PTH	0.062	0.058	1.062	0.289
Transferrin	0.031	0.053	0.589	0.557
BMI	0.024	0.055	0.435	0.664
Phosphate	0.008	0.051	0.155	0.877
IFNγ	0.003	0.06	0.053	0.957
IL-10	0	0.055	-0.007	0.994
IL-1b	-0.028	0.048	-0.590	0.556
Sex	-0.046	0.115	-0.400	0.689
Ferritin	-0.061	0.056	-1.081	0.281
Age	-0.064	0.078	-0.812	0.418
eGFR	-0.087	0.074	-1.167	0.245
1,25(OH)2D	-0.177	0.051	-3.460	0.001

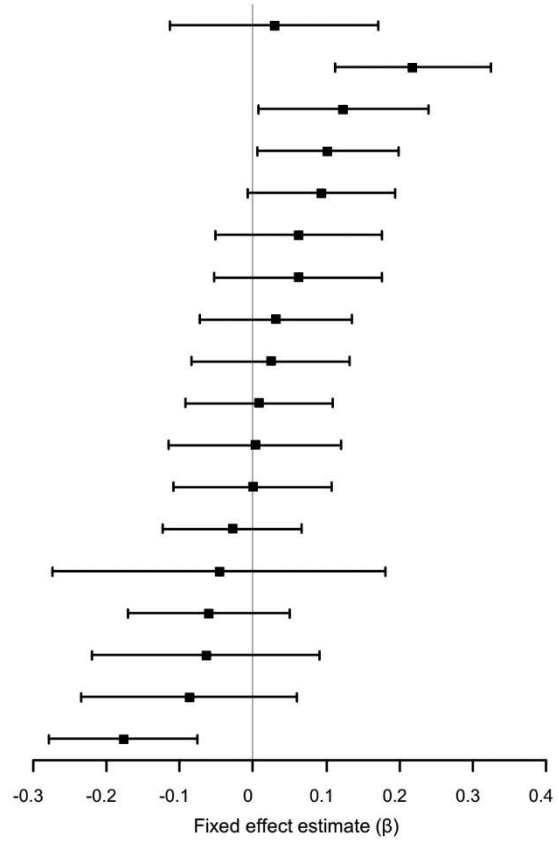

b

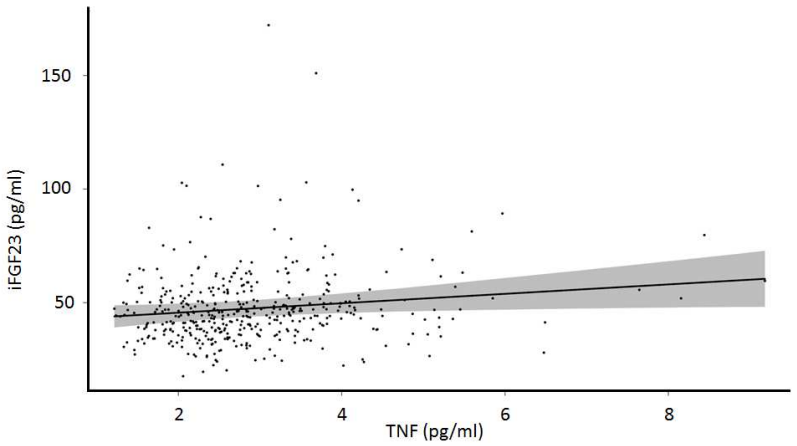

Figure 2

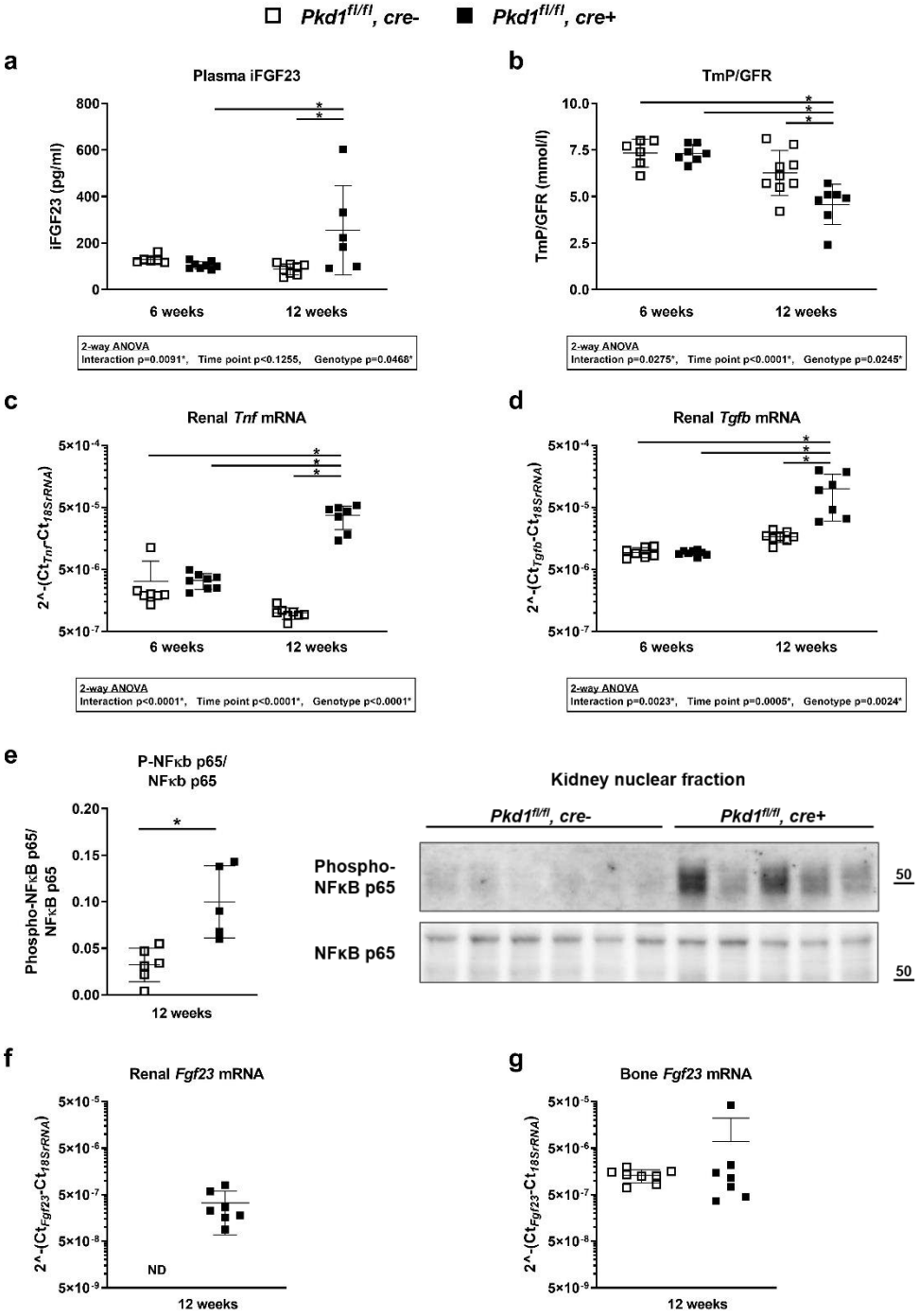
□ Pkd1fl/fl, cre-
■ Pkd1fl/fl, cre+
a
Plasma iFGF23
iFGF23 (pg/ml)
800
600
400
200
0
6 weeks
12 weeks
2-way ANOVA
Interaction p=0.0091*, Time point p<0.1255, Genotype p=0.0468*
b
TmP/GFR
TmP/GFR (mmol/l)
10.0
7.5
5.0
2.5
0.0
6 weeks
12 weeks
2-way ANOVA
Interaction p=0.0275*, Time point p<0.0001*, Genotype p=0.0245*
c
Renal Tnf mRNA
2^-(Ct Tnf-Ct 18S rRNA)
5×10-4
5×10-5
5×10-6
5×10-7
6 weeks
12 weeks
2-way ANOVA
Interaction p<0.0001*, Time point p<0.0001*, Genotype p<0.0001*
d
Renal Tgfb mRNA
2^-(Ct Tgfb-Ct 18S rRNA)
5×10-4
5×10-5
5×10-6
5×10-7
6 weeks
12 weeks
2-way ANOVA
Interaction p=0.0023*, Time point p=0.0005*, Genotype p=0.0024*
e
P-NFκb p65/
NFκb p65
Phospho-NFκB p65/
NFκB p65
0.20
0.15
0.10
0.05
0.00
12 weeks
Kidney nuclear fraction
Pkd1fl/fl, cre-
Pkd1fl/fl, cre+
Phospho-
NFκB p65
NFκB p65
50
50
f
Renal Fgf23 mRNA
2^-(Ct Fgf23-Ct 18S rRNA)
5×10-5
5×10-6
5×10-7
5×10-8
5×10-9
ND
12 weeks
g
Bone Fgf23 mRNA
2^-(Ct Fgf23-Ct 18S rRNA)
5×10-5
5×10-6
5×10-7
5×10-8
5×10-9
12 weeks

Figure 3

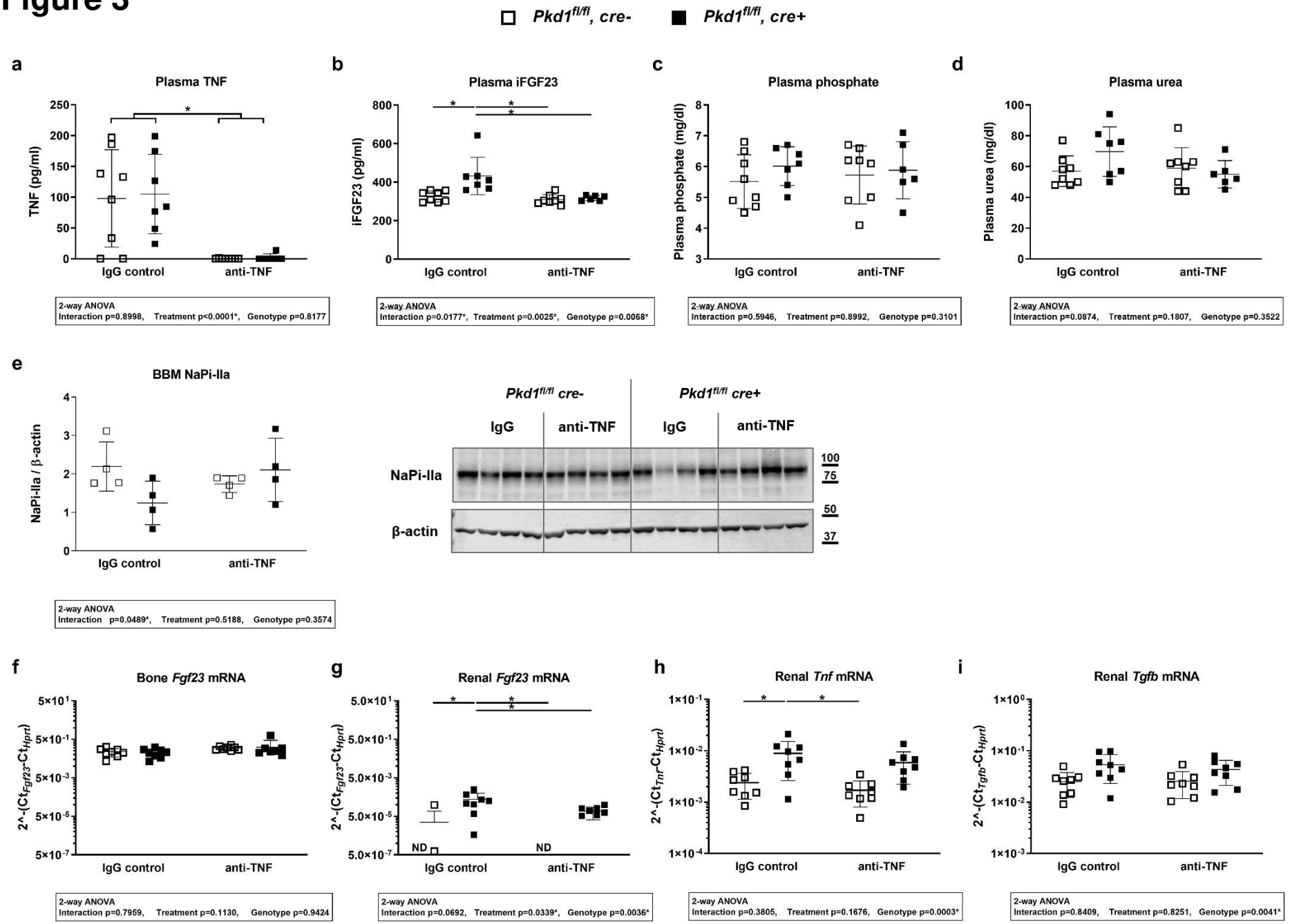
Pkd1fl/fl, cre-
Pkd1fl/fl, cre+
a
Plasma TNF
TNF (pg/ml)
IgG control
anti-TNF
2-way ANOVA
Interaction p=0.8998, Treatment p<0.0001*, Genotype p=0.8177
b
Plasma iFGF23
iFGF23 (pg/ml)
IgG control
anti-TNF
2-way ANOVA
Interaction p=0.0177*, Treatment p=0.0025*, Genotype p=0.0068*
c
Plasma phosphate
Plasma phosphate (mg/dl)
IgG control
anti-TNF
2-way ANOVA
Interaction p=0.5946, Treatment p=0.8992, Genotype p=0.3101
d
Plasma urea
Plasma urea (mg/dl)
IgG control
anti-TNF
2-way ANOVA
Interaction p=0.0874, Treatment p=0.1807, Genotype p=0.3522
e
BBM NaPi-IIa
NaPi-IIa / β-actin
IgG control
anti-TNF
2-way ANOVA
Interaction p=0.0489*, Treatment p=0.5188, Genotype p=0.3574
Pkd1fl/fl cre-
Pkd1fl/fl cre+
IgG
anti-TNF
IgG
anti-TNF
NaPi-IIa
β-actin
100
75
50
37
f
Bone Fgf23 mRNA
2^-(CtFgf23-CtHprt)
IgG control
anti-TNF
2-way ANOVA
Interaction p=0.7959, Treatment p=0.1130, Genotype p=0.9424
g
Renal Fgf23 mRNA
2^-(CtFgf23-CtHprt)
ND
ND
IgG control
anti-TNF
2-way ANOVA
Interaction p=0.0692, Treatment p=0.0339*, Genotype p=0.0036*
h
Renal Tnf mRNA
2^-(CtTnf-CtHprt)
IgG control
anti-TNF
2-way ANOVA
Interaction p=0.3805, Treatment p=0.1676, Genotype p=0.0003*
i
Renal Tgfb mRNA
2^-(CtTgfb-CtHprt)
IgG control
anti-TNF
2-way ANOVA
Interaction p=0.8409, Treatment p=0.8251, Genotype p=0.0041*

Figure 4

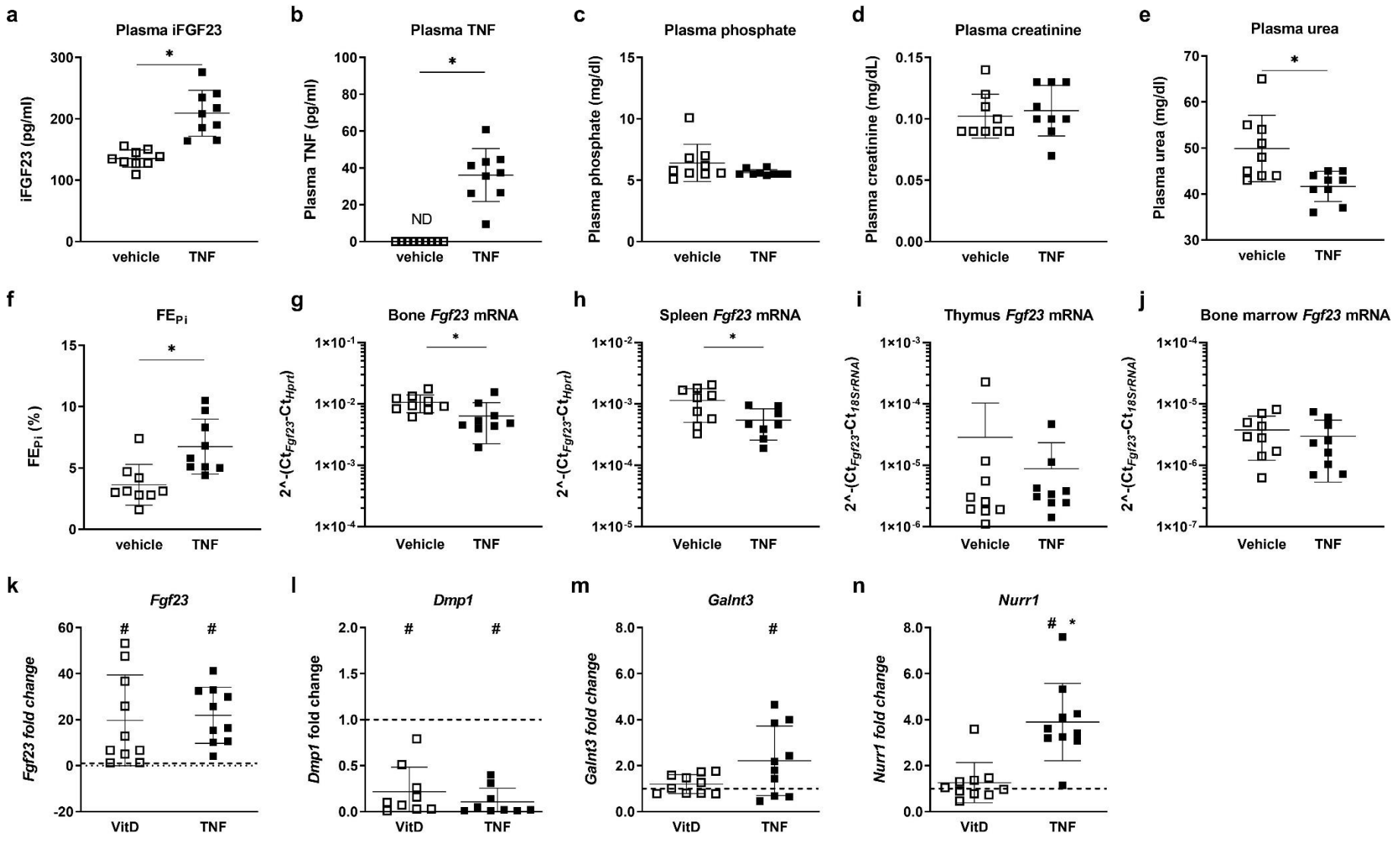
a
Plasma iFGF23
iFGF23 (pg/ml)
300
200
100
0
*
vehicle
TNF
b
Plasma TNF
Plasma TNF (pg/ml)
100
80
60
40
20
0
ND
*
vehicle
TNF
c
Plasma phosphate
Plasma phosphate (mg/dl)
15
10
5
0
vehicle
TNF
d
Plasma creatinine
Plasma creatinine (mg/dL)
0.15
0.10
0.05
0.00
vehicle
TNF
e
Plasma urea
Plasma urea (mg/dl)
70
60
50
40
30
*
vehicle
TNF
f
FEPi
FEPi (%)
15
10
5
0
*
vehicle
TNF
g
Bone Fgf23 mRNA
2^-(CtFgf23-CtHprt)
1×10-1
1×10-2
1×10-3
1×10-4
*
Vehicle
TNF
h
Spleen Fgf23 mRNA
2^-(CtFgf23-CtHprt)
1×10-2
1×10-3
1×10-4
1×10-5
*
Vehicle
TNF
i
Thymus Fgf23 mRNA
2^-(CtFgf23-Ct18SrRNA)
1×10-3
1×10-4
1×10-5
1×10-6
Vehicle
TNF
j
Bone marrow Fgf23 mRNA
2^-(CtFgf23-Ct18SrRNA)
1×10-4
1×10-5
1×10-6
1×10-7
Vehicle
TNF
k
Fgf23
Fgf23 fold change
60
40
20
0
-20
#
#
VitD
TNF
l
Dmp1
Dmp1 fold change
2.0
1.5
1.0
0.5
0.0
#
#
VitD
TNF
m
Galnt3
Galnt3 fold change
8.0
6.0
4.0
2.0
0.0
#
VitD
TNF
n
Nurr1
Nurr1 fold change
8.0
6.0
4.0
2.0
0.0
#
*
VitD
TNF

Figure 5

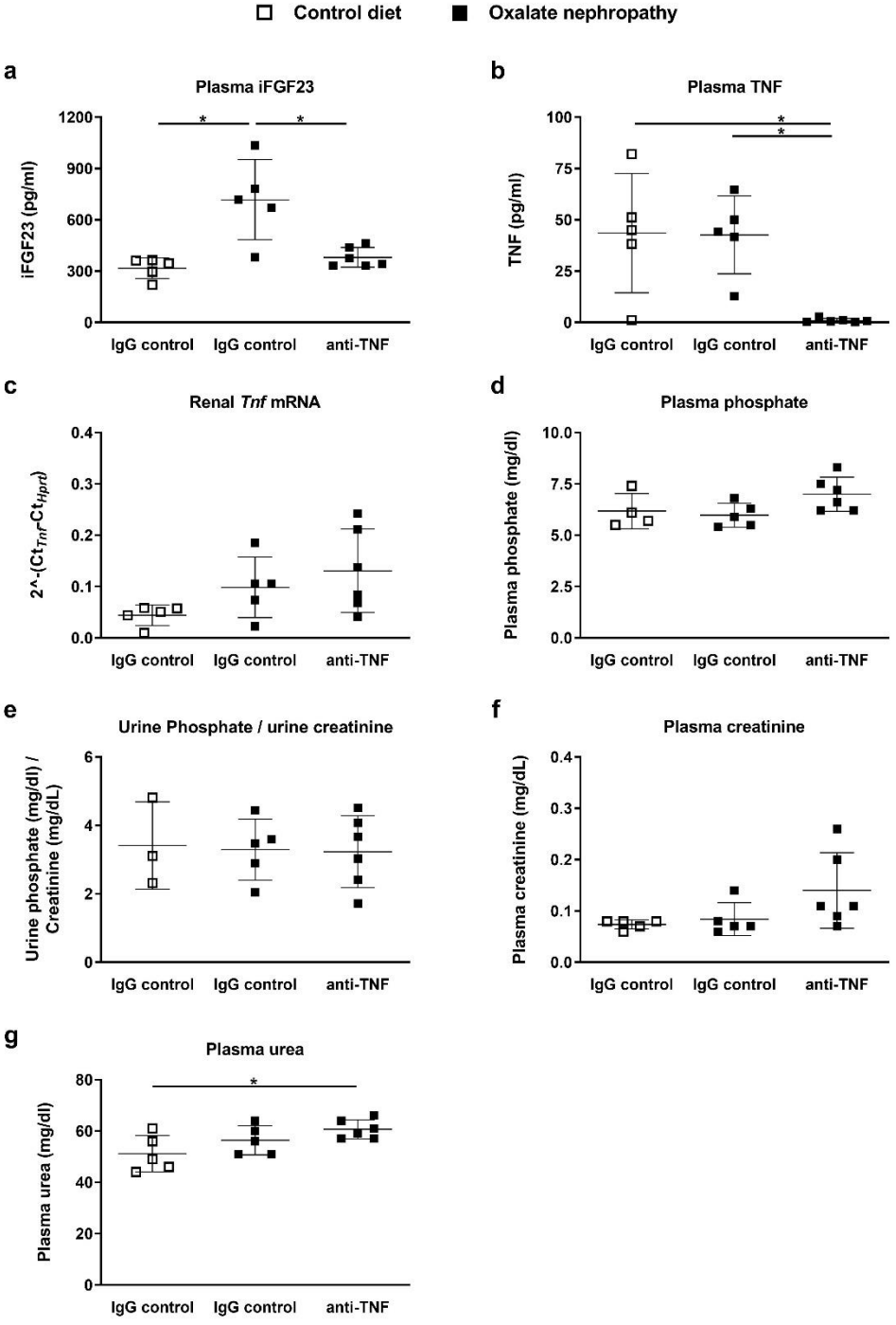
Control diet
Oxalate nephropathy
a
Plasma iFGF23
iFGF23 (pg/ml)
1200
900
600
300
0
*
*
IgG control
IgG control
anti-TNF
b
Plasma TNF
TNF (pg/ml)
100
75
50
25
0
*
*
IgG control
IgG control
anti-TNF
c
Renal Tnf mRNA
2^-(Ct_Tnf-Ct_Hprt)
0.4
0.3
0.2
0.1
0.0
IgG control
IgG control
anti-TNF
d
Plasma phosphate
Plasma phosphate (mg/dl)
10.0
7.5
5.0
2.5
0.0
IgG control
IgG control
anti-TNF
e
Urine Phosphate / urine creatinine
Urine phosphate (mg/dl) / Creatinine (mg/dL)
6
4
2
0
IgG control
IgG control
anti-TNF
f
Plasma creatinine
Plasma creatinine (mg/dL)
0.4
0.3
0.2
0.1
0.0
IgG control
IgG control
anti-TNF
g
Plasma urea
Plasma urea (mg/dl)
80
60
40
20
0
*
IgG control
IgG control
anti-TNF

Figure 6

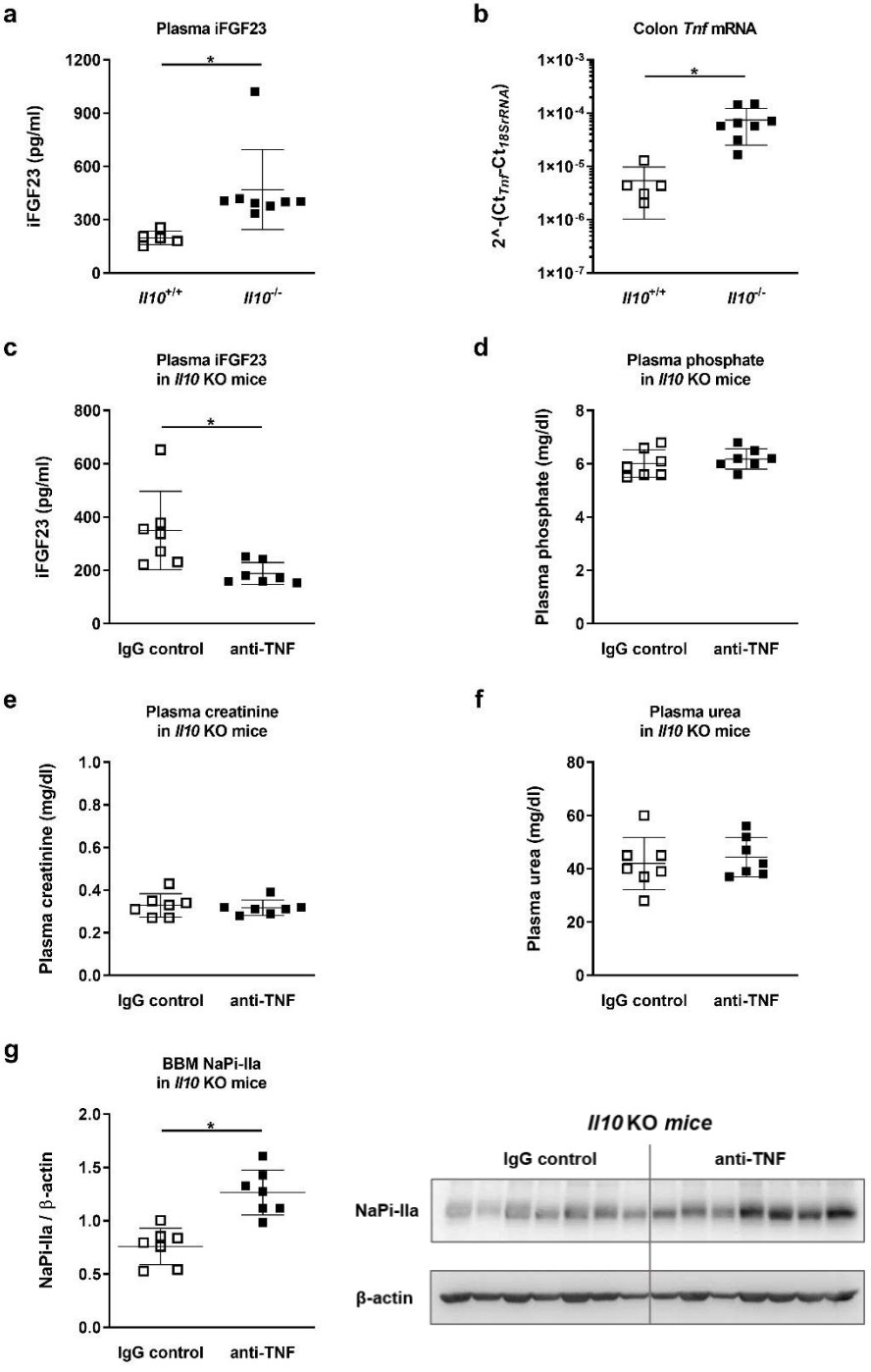
a
Plasma iFGF23
iFGF23 (pg/ml)
1200
900
600
300
0
*
Il10+/+
Il10-/-
b
Colon Tnf mRNA
2^-(CtTnf-Ct18SrRNA)
1×10-3
1×10-4
1×10-5
1×10-6
1×10-7
*
Il10+/+
Il10-/-
c
Plasma iFGF23
in Il10 KO mice
iFGF23 (pg/ml)
800
600
400
200
0
*
IgG control
anti-TNF
d
Plasma phosphate
in Il10 KO mice
Plasma phosphate (mg/dl)
8
6
4
2
0
IgG control
anti-TNF
e
Plasma creatinine
in Il10 KO mice
Plasma creatinine (mg/dl)
1.0
0.8
0.6
0.4
0.2
0.0
IgG control
anti-TNF
f
Plasma urea
in Il10 KO mice
Plasma urea (mg/dl)
80
60
40
20
0
IgG control
anti-TNF
g
BBM NaPi-IIa
in Il10 KO mice
NaPi-IIa / β-actin
2.0
1.5
1.0
0.5
0.0
*
IgG control
anti-TNF
Il10 KO mice
IgG control
anti-TNF
NaPi-IIa
β-actin

a

Without exclusion by drug intake

	β	SE	t-value	p-value
Intercept	0.160	0.13	1.232	0.219
25(OH)D	0.133	0.039	3.373	0.001
TNF	0.053	0.043	1.229	0.220
Calcium	0.111	0.035	3.128	0.002
Iron	0.036	0.037	0.976	0.329
IL-6	0.072	0.044	1.645	0.100
PTH	0.113	0.041	2.725	0.007
Transferrin	0.064	0.038	1.674	0.095
BMI	-0.066	0.042	-1.575	0.116
Phosphate	0.076	0.038	1.976	0.049
IFNγ	-0.013	0.041	-0.309	0.758
IL-10	0.002	0.041	0.054	0.957
IL-1b	-0.026	0.035	-0.745	0.456
Sex	-0.106	0.081	-1.315	0.189
Ferritin	-0.017	0.039	-0.427	0.669
Age	-0.070	0.056	-1.258	0.209
eGFR	-0.122	0.054	-2.245	0.025
1,25(OH)2D	-0.190	0.039	-4.935	0

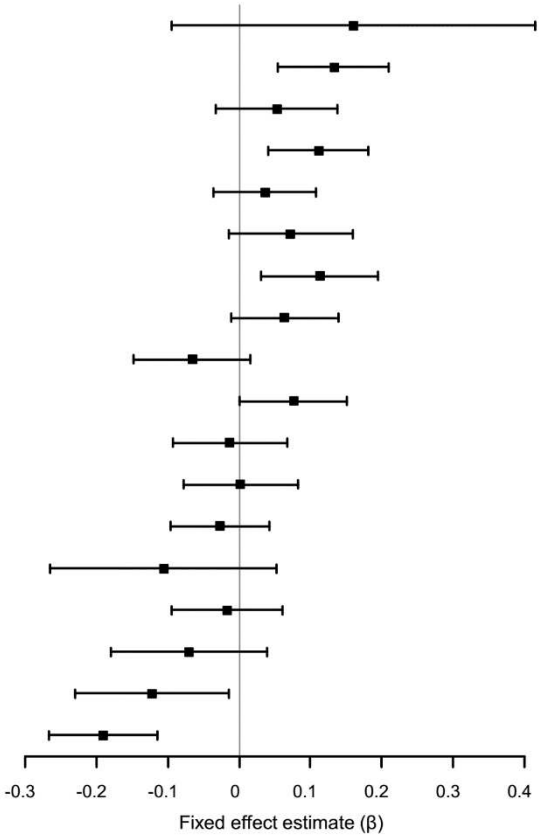

b

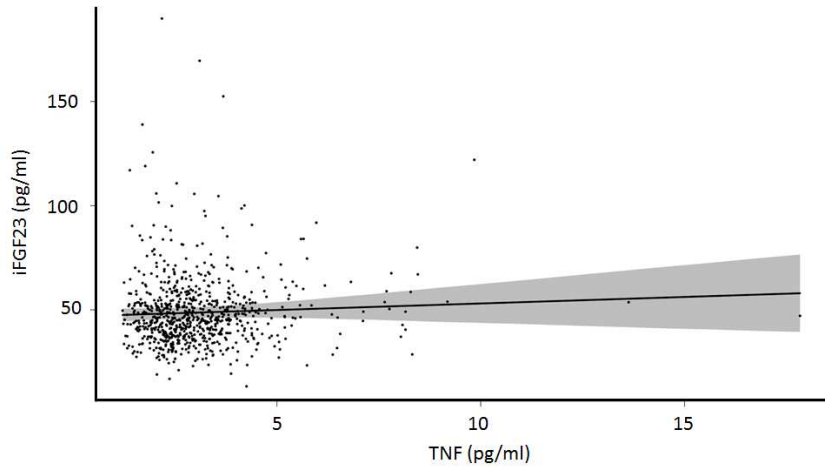

Figure S1

Identification of plasma iFGF23 predictors in a human cohort. (a) Forest plot showing the fixed effects calculated for all predictors used in the mixed linear model for the subpopulation of 790 participants without drug intake criteria applied. Fixed effect estimates (β), standard error, ratio between the estimates and their standard errors (t-value), and associated p-value from a t-distribution. (b) Association between plasma TNF and iFGF23 in the SKIPOGH cohort in a subpopulation of 790 participants after all the exclusion criteria applied. The regression line and confidence band were obtained from the linear mixed model containing all the predictors.

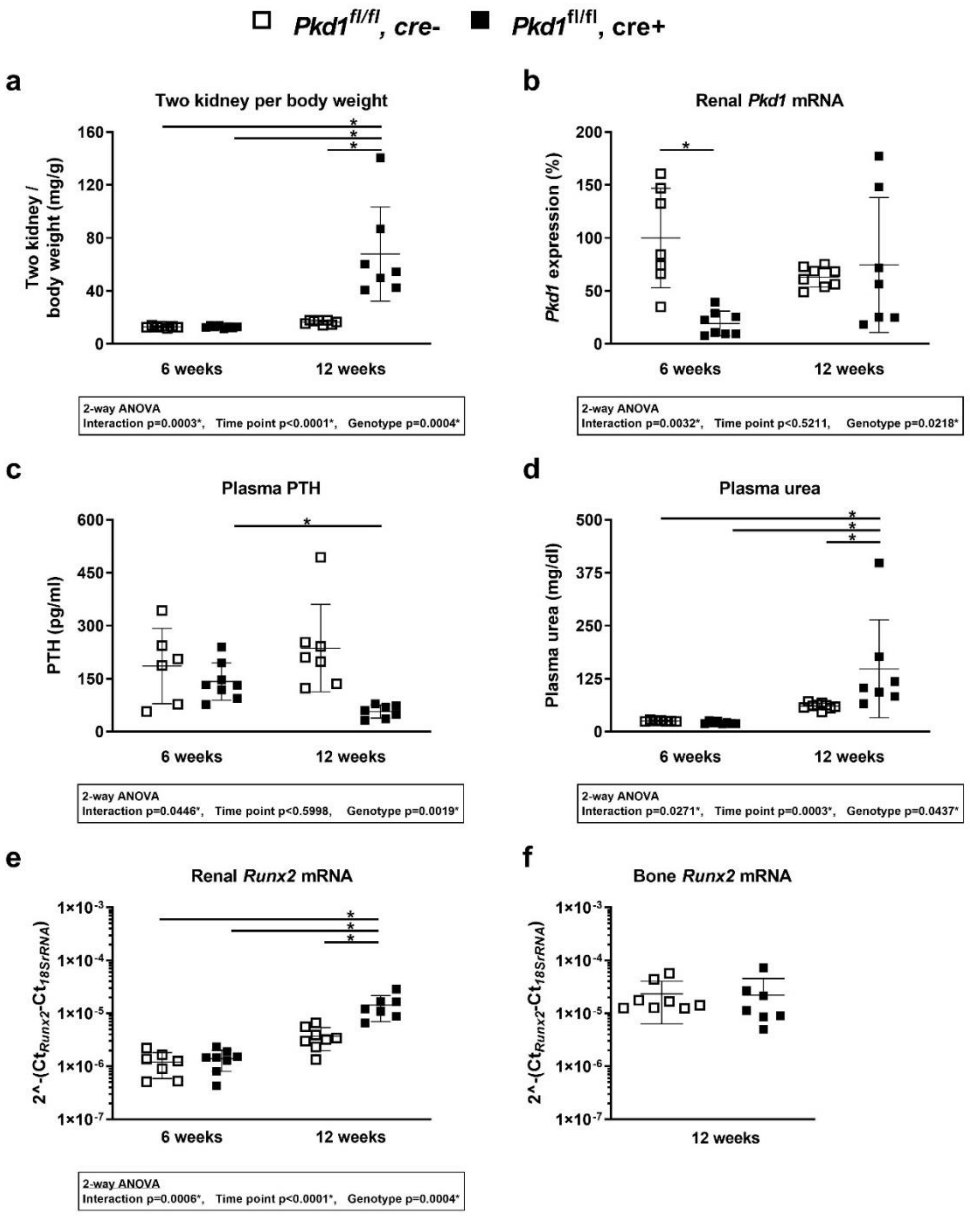

Figure S2

Baseline characteristics of *Pkd1* KO mice. Two-kidney per body weight ratio (a), *Pkd1* gene expression normalized to *Pkd*$^{fl/fl}$*, cre-* mice (6 weeks) (b), plasma iFGF23 (c), plasma PTH (d) and plasma urea (d) as well as *Runx-2* (e, f) mRNA expression relative to 18SrRNA in kidney and bone in *Pkd1*$^{fl/fl}$*, cre-* (white squares) and *Pkd1*$^{fl/fl}$*, cre+* (black squares) animals at the age of 6 and 12 weeks. Two-way ANOVA with Bonferroni correction (a-d, f) or unpaired t-test (e), * $p<0.05$.

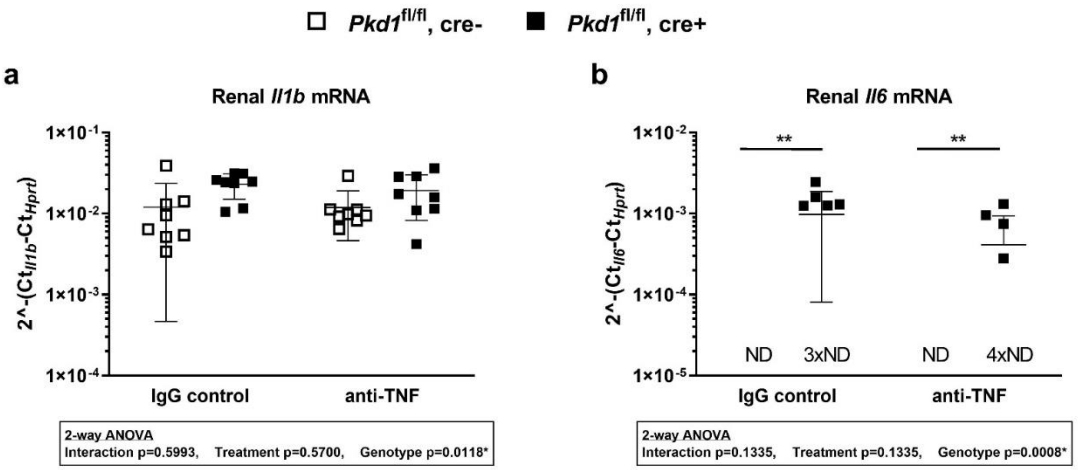

Figure S3

Expression of inflammation markers in the kidney of *Pkd1* KO mice. Renal *Il1b* (a), and renal *Il6* (b) mRNA expression relative to 18SrRNA in *Pkd1$^{fl/fl}$, cre-* (white squares) and *Pkd1$^{fl/fl}$, cre+* (black squares) animals at the age of 6 and 12 weeks. Two-way ANOVA with Bonferroni correction, * $p<0.05$.

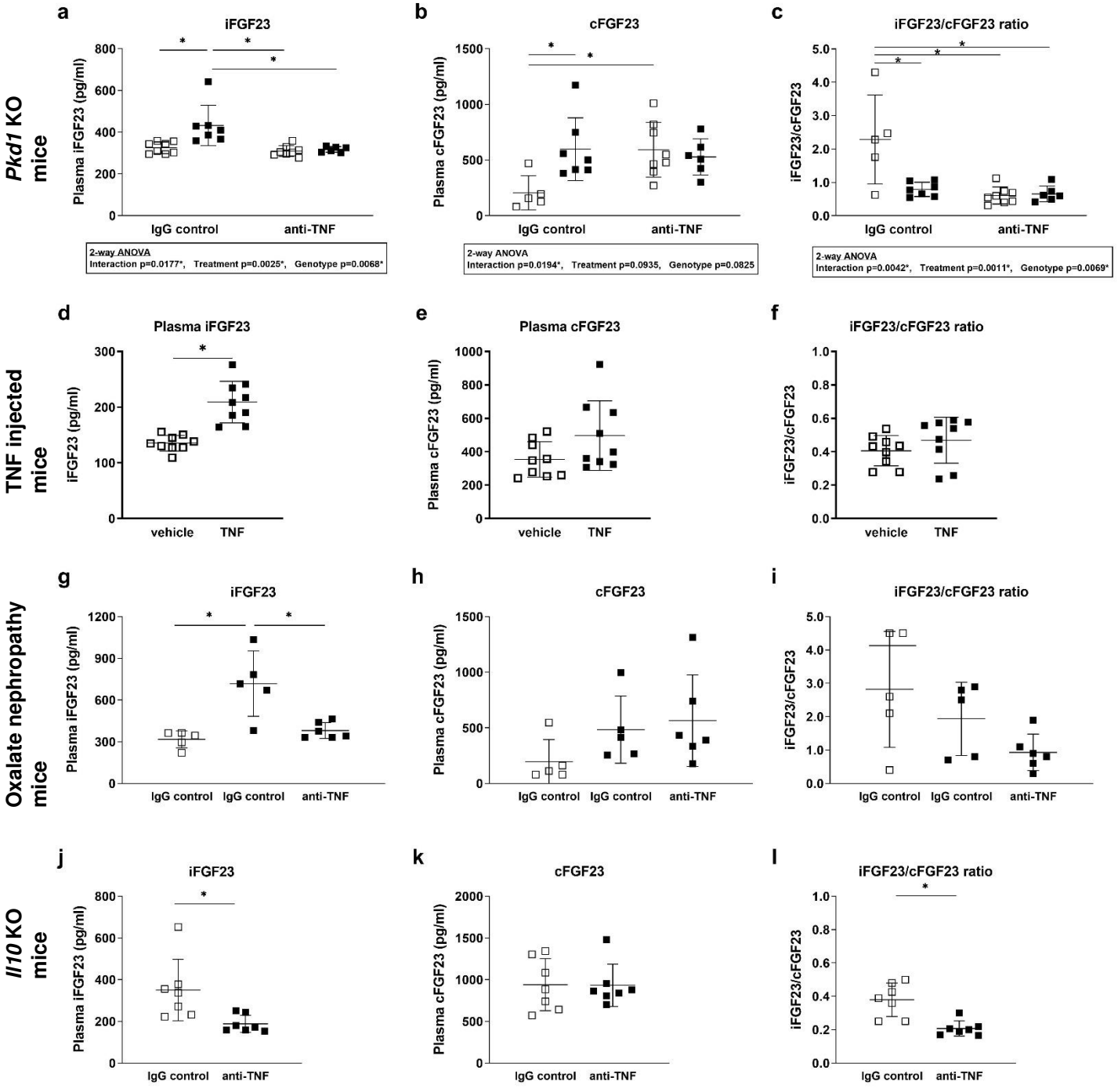

Figure S4

Comparison of plasma iFGF23, cFGF23 and iFGF23 to cFGF23 ratio. Plasma iFGF23 (a, d, g, j), plasma cFGF23 (b, e, h, k) and iFGF23/cFGF23 ratio (c, f, i, l) in *Pkd1* KO mice (*Pkd1*$^{fl/fl}$, *cre-* (white squares) and *Pkd1*$^{fl/fl}$, *cre+* (black squares)), TNF injected mice (2ug/day for two consecutive days), oxalate nephropathy mice (control diet (white squares) and oxalate nephropathy (black squares)). Two-way ANOVA with Bonferroni correction (a-c), One-way ANOVA with Bonferroni correction (g-i) or unpaired t-test (d-f, j-l), * $p<0.05$.

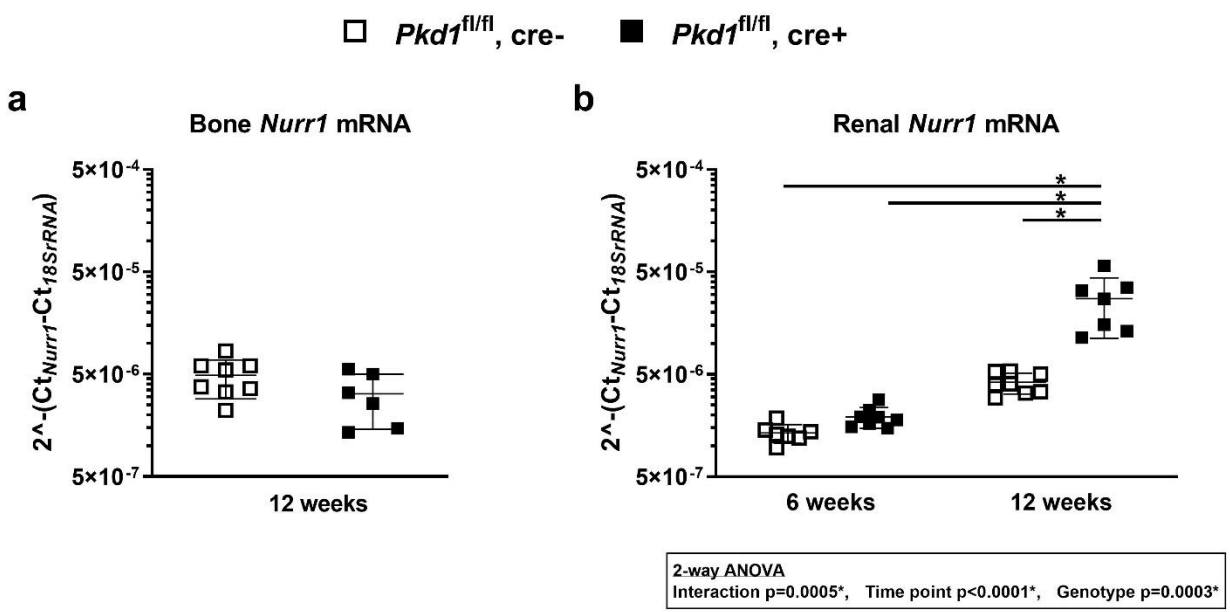

Figure S5

Bone and renal *Nurr1* mRNA expression in *Pkd1* KO mice. *Nurr1* mRNA expression relative to 18SrRNA in kidney (a) and bone (b) in *Pkd1*$^{fl/fl}$*, cre-* (white squares) and *Pkd1*$^{fl/fl}$*, cre+* (black squares) animals at the age of 6 and 12 weeks. Unpaired t-test (a), or Two-way ANOVA with Bonferroni correction (b), * $p<0.05$.

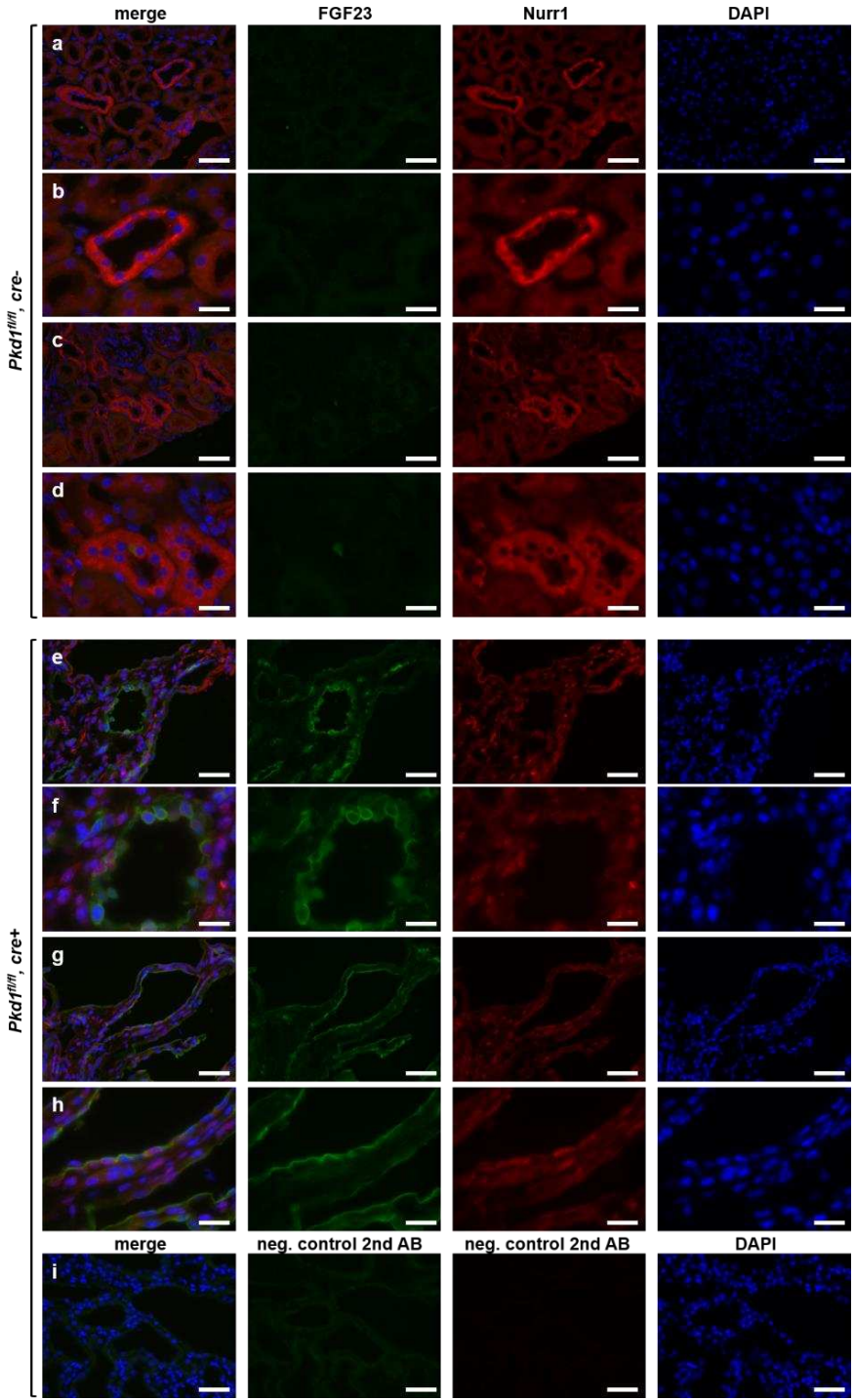

Figure S6

Colocalization of Nurr1 and FGF23 in *Pkd1* kidneys. Immunofluorescence staining for FGF23 (green), Nurr1 (red), and DAPI (blue, cell nuclei) merge and single channels in kidneys of 12 weeks old *Pkd1*$^{fl/fl}$*, cre-* (a-d), *Pkd1*$^{fl/fl}$*, cre+* (e-h) and *Pkd1*$^{fl/fl}$*, cre+* incubated with secondary antibodies alone (i). Original magnification (a, c, e, g) 400x (scale bar 50 µm) and (b, d, f, h) 1000x (scale bar 20 µm).

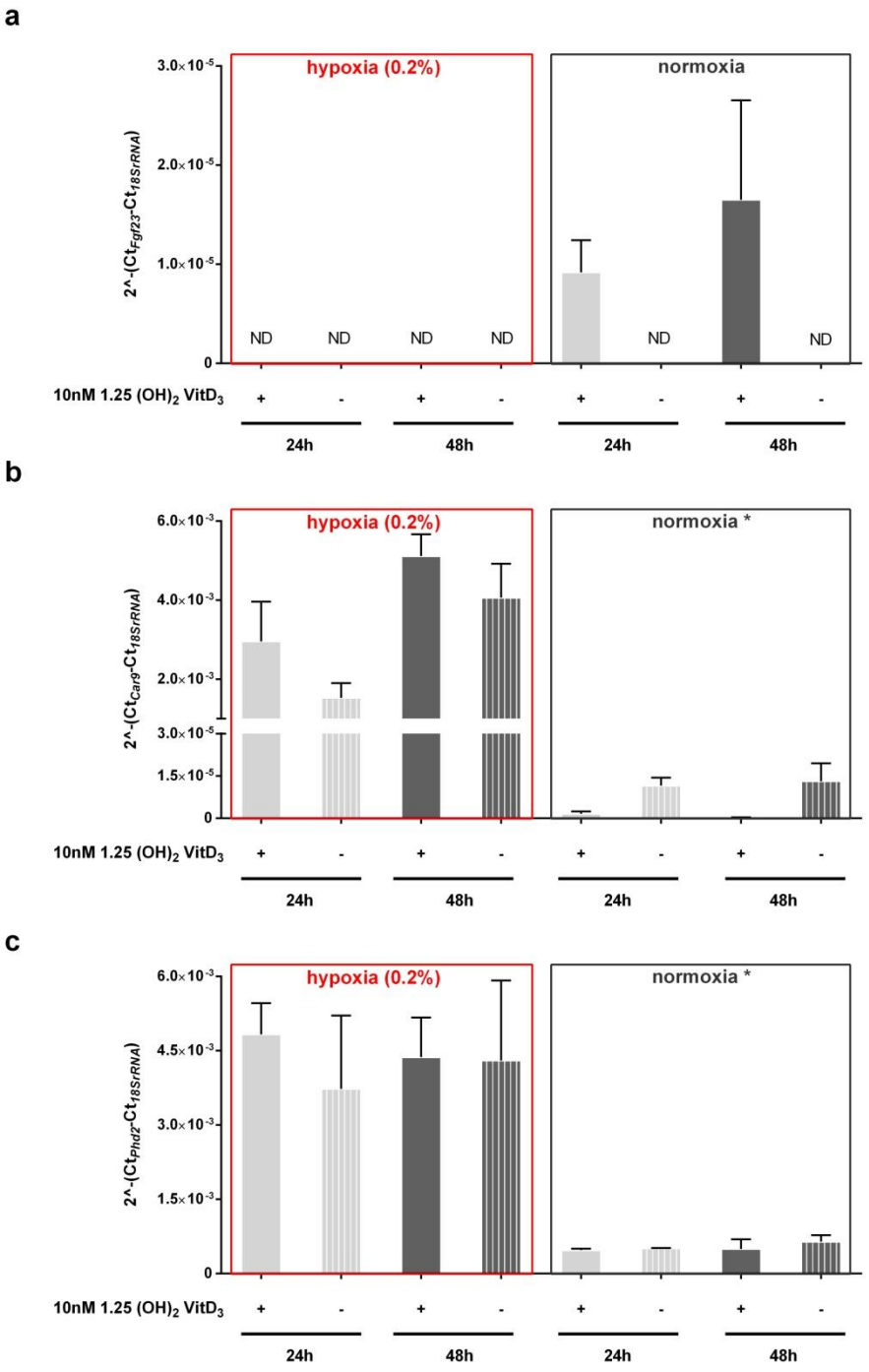

Figure S7

1,25 $(OH)_2$ vitamin D_3 dependent *Fgf23* expression in MC3T3-E1 cells under hypoxic conditions. MC3T3-E1 cells were differentiated for two weeks along the osteogenic lineage. Subsequently, cells were supplemented for 24 or 48 hours with 10nM 1,25 $(OH)_2$ vitamin D_3 and incubated under hypoxic (0.2% oxygen) or normoxic conditions. *Fgf23* (a), *Car9* (b), and *Phd2* (c) mRNA expression relative to 18SrRNA. Mean ±SD; 3 independent experiments; ANOVA with Bonferroni correction, * $p<0.05$.